Journal of Computational Physics **150,** 302–331 (1999)
Article ID jcph.1998.6179, available online at http://www.idealibrary.com on IDEAL®

A Level-Set Approach to the Computation of Twinning and Phase-Transition Dynamics

Thomas Y. Hou,* Phoebus Rosakis,† and Philippe LeFloch‡

*Department of Applied Mathematics, California Institute of Technology, Pasadena, California 91125;
†Department of Theoretical and Applied Mechanics, Cornell University, Ithaca, New York 14853-1503;
and ‡Centre de Mathématiques Appliquées, Centre National de la Recherche Scientifique,
UA756 Ecole Polytechnique, 91128 Palaiseau Cedex, France
E-mail: *hou@ama.caltech.edu, †phoebus@cornell.edu, and ‡lefloch@cmapx.polytechnique.fr

Received July 24, 1998; revised December 21, 1998

A computational method is proposed for the dynamics of solids capable of twinning and phase transitions. In a two-dimensional, sharp-interface model of twinning, the stored-energy function is a nonconvex potential with multiple wells. The evolution of twin interfaces is governed by field equations and jump conditions of momentum balance, and by a kinetic relation expressing the interface velocity as a function of the local driving traction and interfacial orientation. A regularized version of the model is constructed based on the level-set method. A level-set function which changes signs across the interface is introduced. The evolution of this function is described by a Hamilton–Jacobi equation, whose velocity coefficient is determined by the kinetic relation. Jump conditions are thereby eliminated, allowing finite-difference discretization. Numerical simulations exhibit complex evolution of the interface, including cusp formation, needle growth, spontaneous tip splitting, and topological changes that result in microstructure refinement. The results capture experimentally observed phenomena in martensitic crystals.

0. INTRODUCTION

We present a new numerical method for the computation of propagating interfaces in solid materials, such as crystals undergoing twinning, or shape-memory alloys capable of phase transitions of austenite–martensite type. Phase boundaries propagate in crystalline solids at subsonic speeds that cannot be determined solely from the constitutive law and the balance laws of continuum mechanics. Various models of phase-boundary propagation involve a coupling of field equations and jump conditions on evolving discontinuity surfaces, which is not amenable to the use of standard computational techniques. The present paper represents an effort to overcome such difficulties.

0021-9991/99 $30.00

Many crystalline solids admit multiple phases. Each phase is associated with a distinct crystal symmetry type or orientation of the lattice. The experimentally observed mechanical behavior of shape-memory alloys is quite complex. Under a suitable combination of thermal and mechanical loading, they develop spatially complex *microstructures*. These comprise a collection of *phase boundaries* between regions of the body in different phases, or *twin interfaces* between differently oriented twin lattice variants. Although the behavior within each phase or variant is often essentially elastic, interface evolution is accompanied by energy dissipation. As a result, the overall mechanical response of these materials is hysteretic. In biaxial loading experiments in a Cu–Al–Ni single crystal, Chu and James [9] observed laminated twinned microstructures forming in the martensitic phase. Different regions were occupied by collections of parallel twin layers. These bands taper down to needlelike tips, sometimes in the interior, but usually when they encounter the boundary of a differently oriented laminate. Evolution of this microstructure under load changes is complex. It involves largely longitudinal growth of needles, combined with sudden *splitting* of needle tips, that frequently leads to complete separation of a twin band into finer needles [1, 9] and results in overall microstructure refinement.

The stored-energy function for such a solid can be modeled as a nonconvex multiwell function. Each well corresponds to a preferred deformation state associated with a specific phase of the material. Various studies of static microstructural morphology focus on the variational problem of global minimization of the total energy functional (e.g., [6, 18, 24]). They predict energy-minimizing configurations that typically involve microstructures with fine-scale mixtures of two or more phases. These capture many observed features of microstructure morphology in static situations. On the other hand, time-dependent behavior under applied loads cannot be fully understood by energy minimization, as it is not energetically conservative and involves inertia effects. In addition, local energy minima, which may be physically relevant [1], cannot be identified in this fashion.

In order to understand evolving phase transitions, a number of models for continuum dynamics of transforming materials were developed. They all share the basic balance laws of continuum mechanics as a starting point. These conservation laws are of mixed type; that is, the underlying partial differential equations change from hyperbolic to elliptic, depending on local properties of the solution. This is due to nonconvexity of the stored-energy function. Traveling discontinuities arise naturally in this setting and are governed by Rankine–Hugoniot jump conditions. They are called *shocks* when they separate states in the same phase or *phase boundaries* when the states on either side are in different phases. Both kinds give rise to dissipation when in motion. Dynamic problems involving phase boundaries suffer from a massive loss of uniqueness of solutions: in contrast to shocks, the propagation speed of these fronts is not completely determined by momentum balance (see, e.g., [17].) The imposition of the second law of thermodynamics (Clausius–Duhem inequality) fails to select a unique solution in general, although it rejects some that are physically unacceptable. As a result, an additional constitutive criterion is needed for the determination of interface dynamics. The following approaches to that effect have been proposed:

Various ways of regularization of the underlying PDEs augment the constitutive law by including additional effects, such as *viscosity* and *higher-order gradients*. In these models, a sharp interface is replaced by a transition layer with internal structure (e.g., [4, 5, 11, 16, 31, 32]).

Alternatively, *phase-field models* introduce an additional field variable—the order parameter—that describes the location and structure of the phase-transition layer. This new

variable satisfies an equation of Ginzburg–Landau type involving a two-well potential among other terms. This is coupled to the momentum-balance equation (see, for instance, [7, 13]).

Finally, in the *sharp-interface theory*, interfaces are treated as discontinuity surfaces of zero thickness. Additional constitutive information is prescribed for them. In the simplest such theory, the energy dissipation is found to equal the product of the normal interface velocity and the *driving traction*. The latter is determined by the local states on either side of the interface. The model introduces a constitutive *kinetic relation* that determines the velocity as a function of the driving traction (and possibly of other variables) [2, 3, 12, 21, 28, 33, 34]. More complex theories prescribe, in addition, interfacial stress and energy [15].

It is worth noting that diffuse-interface theories of the first two kinds select a *specific* kinetic relation for the sharp-interface model that they approach in a suitable asymptotic limit [4, 13]. For one-dimensional elastic bars, Abeyaratne and Knowles [3] establish well-posedness of the Riemann problem when a kinetic relation is specified; a *nucleation criterion* is also prescribed and determines the onset of phase change. More general initial data are treated by LeFloch [21].

For definiteness, we focus on a two-dimensional, sharp-interface model for dynamic twinning processes in body-centered cubic (anisotropic) crystals. In Section 1 we review the dynamic field equations and jump conditions. Section 2 describes specific constitutive choices. Generalizing the approach of Abeyaratne and Knowles [3], we adopt a kinetic relation for the twin interfaces that takes *interfacial orientation* into account. This *anisotropic* kinetic relation determines the normal interface velocity at each point as a specific function of the driving traction and the interface unit normal. A more detailed treatment, as well as analytical solutions for specific simple problems, may be found in [26, 27] for the case of statics and in [28, 34] for the dynamic case.

The development of computational algorithms for evolving interfaces poses an important challenge. Standard shock-capturing schemes and finite-element methods cannot be applied directly to the sharp-interface model. For classical fluid dynamics problems, it is known that difference schemes consistent with the conservation form of the equations converge to weak (discontinuous) solutions of the PDEs. This result is not pertinent for phase-transition problems, due to the indeterminacy of phase-boundary motion. Phase interfaces turn out to be very sensitive to numerical dissipation, regularization, and mesh refinement.

The challenge is therefore to design numerical schemes that are consistent with a given, independently assigned interfacial kinetic relation. This should be done in a way that ensures convergence of the numerical solution to that of the sharp-interface problem as the mesh size approaches zero. The interface should be driven by the given kinetic relation rather than by artificial numerical dissipation.

A numerical algorithm that meets these requirements was proposed by Zhong *et al.* [37]. Therein phase boundaries were tracked and discontinuities captured by a high-order Godunov-type scheme. This method is quite efficient in one-dimensional problems with a limited number of interfaces. For higher-dimensional problems, the front-tracking techniques developed for computational fluid dynamics by Glimm *et al.* [14], and also by LeVeque and Shyue [22], could be adapted in principle. However, tracking interfaces with complex geometry in higher dimensions leads to considerable numerical difficulty. This problem is avoided by the method we propose below.

The *level-set formulation* for evolving curves or surfaces was introduced by Osher and Sethian [25] in a computational method for curvature-driven interfaces. The main

advantage of this approach is that it can handle singularity formation (corners or cusps), self-intersection, topological changes, and the formation of complex interface geometry with no additional computational complexity. Such phenomena are typically encountered in twinned microstructure evolution.

The evolution of interfaces driven solely by curvature is independent of processes taking place elsewhere in the bulk. Recently, the level-set approach was extended to situations where bulk processes are coupled to the interface in some way. For instance, the interface between two distinct Newtonian fluids interacts with the Navier–Stokes bulk flow through convection and surface tension in studies by Sussman *et al.* [30] and Chang *et al.* [8]. The twinning problem studied in this paper involves interfacial coupling through kinetics and momentum balance to an elastodynamic process in the bulk material.

In Section 3, we develop an alternative level-set formulation of the twinning problem by introducing an additional *level-set function* φ. The interface is viewed as the zero level set of φ. In order to avoid discontinuities in computation, the interface is replaced by a transition layer containing all points where $|\varphi| < \varepsilon$. Here ε is a small regularization parameter that controls interface thickness. Outside this layer, the field equations of the sharp-interface model are maintained, while within it, the stored-energy function undergoes a smooth transition from a low-strain branch to a high-strain branch. The regularized driving traction, now defined on the entire domain, is obtained from a dissipation-rate calculation analogous to the one for sharp interfaces. The level-set function φ evolves according to a Hamilton–Jacobi equation of the general form $\varphi_t - V|\nabla\varphi| = 0$. Here V, the normal velocity of level sets of φ, is delivered by the kinetic relation. This allows us to arbitrarily select any kinetic relation from the sharp-interface model. In contrast, in theories of the viscosity–capillarity type, the regularization enforces a particular form of the kinetics that cannot be altered. A specific model is described in detail in Section 4.

To some extent, our formulation is analogous to the phase-field models constructed by Fried and Gurtin [13]. The role played by the level-set function is similar to that of an order parameter. However, our approach is an attempt to mimic the sharp-interface model, without introducing additional physics (to the extent allowed by regularization). In particular, we do not include explicit interfacial and exchange energies as it is done in [13].

A finite-difference discretization of the level-set formulation is presented in Section 5. Section 6 describes the results of a number of simulations with emphasis on morphological evolution of the twin interface. Various interesting phenomena are observed. These include needle and cusp formation from an initially smooth interface, spontaneous tip splitting after twin needles reach the boundary, and topological changes where a twin zone separates into two disjoint regions. All of these phenomena illustrate an important mechanism for microstructure evolution and refinement; they bear a strong resemblance to the experimental observations of [1, 9].

1. SHARP-INTERFACE THEORY

As shown in [27, 34] many aspects of twinning deformations in body-centered cubic crystals can be described in the setting of anti-plane shear, which we employ here. A discussion of dynamic anti-plane shear can be found in [28]. We adopt a two-dimensional description. Boldface letters denote vectors in $\mathbb{R}^2$. Consider a body which occupies a cylindrical region with open-bounded cross section $\Omega \subset \mathbb{R}^2$. *Anti-plane shear* motions (time-dependent deformations) are described by the scalar *out-of-plane displacement* field $u(\mathbf{x}, t)$

for $\mathbf{x} = (x, y) \in \Omega$, $t \geq 0$; its physical meaning is given in [27, 28]. The displacement u is assumed continuous and piecewise smooth. The *shear-strain vector*

$$\gamma = \nabla u = (u_x, u_y) \tag{1.1}$$

and the particle velocity u_t suffer jump discontinuities across certain *interfaces*, that is, time-dependent curves $\Gamma_t \subset \Omega$.

The global, or weak, form of *linear momentum balance* involves the shear-stress vector $\boldsymbol{\sigma}$, the acceleration u_{tt}, and the constant mass density $\rho > 0$. It requires that for any subregion $P \subset \Omega$,

$$\int_{\partial P} \boldsymbol{\sigma} \cdot \mathbf{n}\, ds = \int_P \rho u_{tt}\, dA. \tag{1.2}$$

The constitutive relation of a hyperelastic material supplies the stress vector as the gradient of the *stored-energy function* $W(\gamma)$:

$$\boldsymbol{\sigma} = \frac{\partial W}{\partial \gamma}. \tag{1.3}$$

The essential ingredient of most models of phase transformations and twinning is a nonconvex W with multiple potential wells. For the simplest description of twinning [26–28] it suffices to view W as a two-well potential

$$W(\gamma) \geq W(\mathbf{0}) = W(\boldsymbol{\xi}) = 0 \qquad \text{for all } \gamma \in \mathbb{R}^2, \tag{1.4}$$

with global minima (wells) at $\gamma = \mathbf{0}$ and $\boldsymbol{\xi}$, where $\boldsymbol{\xi} = \text{const.}$ is the twinning shear vector. We assume that there are two *disjoint* regions of strain S_i, $i = 0, 1$, where W is strictly convex, with $\mathbf{0} \in S_0$ and $\boldsymbol{\xi} \in S_1$. We refer to S_0 and S_1 as the *low-strain phase* and *high-strain phase*, respectively. Convexity fails for strains outside S_i. For simplicity we set

$$W(\gamma) = \begin{cases} W_0(\gamma) & \text{for } \gamma \in S_0, \\ W_1(\gamma) & \text{for } \gamma \in S_1, \end{cases} \tag{1.5}$$

where W_0 and W_1 are globally defined strictly convex functions achieving their global minimum at $\mathbf{0} \in S_0$ and $\boldsymbol{\xi} \in S_1$, respectively. The details of these functions embody crystallographic and other characteristics of the material which are discussed in detail in [27]. Stability considerations rule out strains where W is nonconvex as physically unattainable. This means that at each instant the domain is separated into two time-dependent subsets $\Omega_t^{\pm}$, such that strains are in the low-strain phase S_0 in Ω_t^- and in the high-strain phase S_1 in Ω_t^+. In particular, $W = W_0$ in Ω_t^-, while $W = W_1$ in Ω_t^+.

The *interface* or twin boundary $\Gamma_t = \Omega_t^+ \cap \Omega_t^-$ consists of piecewise-smooth curves that separate the part of the body that is in the low-strain phase from that in the high-strain phase. The unit normal to Γ_t may suffer discontinuities at isolated points; this allows for needlelike boundaries observed in twinning [9, 27]. Strain and velocity discontinuities occur across Γ_t, while $|\nabla u| \in S_0 \cup S_1$ on $\Omega - \Gamma_t$. In general, Γ_t may evolve and change shape. The motion of interfaces is determined by specifying the (scalar) *normal velocity* $V = V(\mathbf{x}, t)$ at each point $\mathbf{x}$ of Γ_t and time t.

The jumps in strain and velocity across Γ_t are restricted by the continuity of u to obey the jump conditions [2, 28]

$$[\![\nabla u]\!] \cdot \mathbf{t} = 0, \tag{1.6}$$

$$[\![u_t]\!] + V[\![\nabla u]\!] \cdot \mathbf{n} = 0. \tag{1.7}$$

Here $[\![\psi]\!] = \psi^+ - \psi^-$ is the jump of any field ψ across Γ_t; the $+$ and $-$ superscripts indicate limits as Γ_t is approached from $\Omega_t^{\pm}$; $\mathbf{n}$ and $\mathbf{t}$ are the unit normal and tangent to Γ_t, respectively, with $\mathbf{n}$ pointing into Ω^-. At points where u is smooth one may employ a localization argument to reduce the global momentum-balance law (1.2) to the equation of motion

$$\nabla \cdot \boldsymbol{\sigma} = \rho u_{tt} \qquad \text{on } \Omega - \Gamma_t. \tag{1.8}$$

At points on the interface Γ_t localization of (1.2) yields a momentum jump condition [2, 28]

$$[\![\boldsymbol{\sigma}]\!] \cdot \mathbf{n} + V\rho[\![u_t]\!] = 0 \qquad \text{on } \Gamma_t. \tag{1.9}$$

Apart from the interface Γ_t, discontinuities may also occur within each of the regions $\Omega^{\pm}$. These are *shock waves* and they are subject to the above jump conditions (1.6), (1.7), and (1.9) as well. However, they differ from interfaces; strains on either side of a shock wave are in the same phase.

The motion of shock waves and interfaces is accompanied by energy dissipation. The *dissipation rate* $\Delta(t)$ is the excess of the rate of external work over the rate of change of stored elastic and kinetic energy; it is required to be nonnegative by virtue of a suitable version of the second law of thermodynamics [2]:

$$\Delta(t) = \int_{\partial\Omega} u_t \boldsymbol{\sigma} \cdot \mathbf{n}\, ds - \frac{d}{dt}\int_{\Omega}\left(W + \frac{1}{2}\rho u_t^2\right) dA \geq 0. \tag{1.10}$$

Abeyaratne and Knowles [2] show that

$$\Delta(t) = \int_{\Gamma_t} f V\, ds, \tag{1.11}$$

where f is called the *driving traction* acting on the moving interface Γ_t and V is the normal velocity of Γ_t. In the present setting the driving traction takes the form [28]

$$f = -[\![W]\!] + \frac{1}{2}[\![\nabla u]\!] \cdot (\boldsymbol{\sigma}^+ + \boldsymbol{\sigma}^-) \qquad \text{on } \Gamma_t. \tag{1.12}$$

It follows from the localization of (1.11) that the following dissipation inequality must hold,

$$fV \geq 0 \qquad \text{on } \Gamma_t. \tag{1.13}$$

In one-dimensional problems involving a single material phase—hence only shock waves—the field equations and jump conditions analogous to the above suffice for uniqueness of solutions to suitable initial-boundary-value problems, provided the dissipation inequality (1.13) is enforced. In contrast, the presence of interfaces separating different material phases results in a massive loss of uniqueness [17]. It is by now well understood

(e.g., [3, 21]) that additional constitutive information is needed in order to characterize the evolution of interfaces. In one dimension, this may take the form of a *kinetic relation*, $V = g(f)$, between the rate of phase transformation (speed of the interface V) and the driving traction f. Abeyaratne and Knowles [2, 3] show that such a criterion selects a unique solution to the Riemann problem. Tsai [34] and Rosakis and Tsai [28] generalize this approach to possibly curved twin boundaries in two dimensions. Following those studies, we postulate that there exists a *kinetic relation*, which determines the normal velocity V at each point of Γ_t in terms of the local driving traction f and—in addition—the unit normal $\mathbf{n}$ to the interface Γ_t at that point. Specifically, we postulate

$$V = g(f, \mathbf{n}) \qquad \text{on } \Gamma_t, \tag{1.14}$$

where g is the *kinetic response function* characteristic of the material. The explicit dependence on the local boundary orientation through the normal $\mathbf{n}$ takes into account the anisotropy of the material. The kinetic response function g is required to satisfy

$$fg(f, \mathbf{n}) \geq 0 \tag{1.15}$$

for all values of f and all unit vectors $\mathbf{n}$, so that it is consistent with the dissipation inequality (1.13).

2. A SPECIFIC MODEL FOR TWINNING

We adopt a constitutive model (Rosakis and Tsai [28]; Tsai [34]) originally developed to describe twinning deformations in body-centered cubic crystals. For simplicity the stored-energy function of each phase in (1.5) is chosen to be quadratic:

$$W_0(\gamma) = \frac{\mu}{2}|\gamma|^2, \qquad W_1(\gamma) = \frac{\mu}{2}|\gamma - \boldsymbol{\xi}|^2. \tag{2.1}$$

The constant $\mu > 0$ is the shear modulus. For the constitutive law specified above, the stress-strain relation is found from (1.3) and (2.1). It is *linear* in each phase:

$$\boldsymbol{\sigma}(\gamma) = \begin{cases} \boldsymbol{\sigma}^0(\gamma) = \mu\gamma & \text{on } \Omega_t^-, \\ \boldsymbol{\sigma}^1(\gamma) = \mu(\gamma - \boldsymbol{\xi}) & \text{on } \Omega_t^+. \end{cases} \tag{2.2}$$

The equation of motion (1.8) then reduces to the wave equation

$$\Delta u = \frac{1}{c^2} u_{tt} \qquad \text{on } \Omega - \Gamma_t, \tag{2.3}$$

valid away from the interface. The constant $c = \sqrt{\mu/\rho}$ is the *shear wave speed*. For the special material at hand there are two kinds of traveling discontinuities. For *shock waves* the strains on either side of the discontinuity belong to the same phase. It can be shown from the jump conditions (1.6), (1.7), (1.9) that the normal velocity V must equal the shear wave speed c. Thus shock waves reduce to ordinary elastic shear waves for this special model, as a consequence of the linearity of the stress–strain relation in each phase. Another possibility is that the strains on either side of Γ_t belong to different phases. Then

the jump conditions (1.6), (1.7), (1.9) dictate that $V < c$. The jump conditions now reduce to [28]

$$[\![\nabla u]\!] = \frac{(\boldsymbol{\xi}\cdot\mathbf{n})\mathbf{n}}{1 - V^2/c^2} \qquad \text{on } \Gamma_t, \tag{2.4}$$

determining the strain jump across Γ_t in terms of the normal velocity V and the normal $\mathbf{n}$. Such a Γ_t is called a subsonic *twin interface*. The linearity of the stress response inside each phase dictates that $f = 0$; hence elastic shear waves are dissipation free. In contrast, the driving traction on twin interfaces does not vanish in general; one finds from (1.12) and (2.2)

$$f = \frac{1}{2}\boldsymbol{\xi}\cdot[\boldsymbol{\sigma}^1(\gamma^+) + \boldsymbol{\sigma}^0(\gamma^-)] = \frac{\mu}{2}\boldsymbol{\xi}\cdot(\nabla u^+ + \nabla u^- - \boldsymbol{\xi}) \qquad \text{on } \Gamma_t. \tag{2.5}$$

A specific form of kinetic relation was considered in [28]. For simplicity let $\boldsymbol{\xi} = (0, \xi)$. Then, letting $\mathbf{n} = (n_1, n_2)$, choose in (1.14)

$$V = g(f, \mathbf{n}) = Mf|n_1|, \tag{2.6}$$

where the constant $M > 0$ is a mobility coefficient. The motivation for this special type of anisotropic orientation dependence is discussed in detail in [28, 34]. It arises from a dislocation model of the interface. It is to be compared with the more common isotropic kinetic relation $V = Mf$, which does not depend on interfacial orientation. The latter gives rise to interface morphologies that are not observed experimentally.

The *sharp-interface dynamic problem* consists of seeking a solution u of (2.3) subject to the jump condition (2.4) on the moving curve Γ_t. The evolution of Γ_t is to be determined from a kinetic relation (1.14), such as the specific form (2.6), with f supplied by (2.5). Initial conditions involve specification of

$$u(\mathbf{x}, 0) = u_0(\mathbf{x}); \qquad u_t(\mathbf{x}, 0) = v_0(\mathbf{x}) \quad \text{for } \mathbf{x} \in \Omega; \qquad \Gamma_{t=0} = \Gamma_0; \tag{2.7}$$

here Γ_0 is the initial interface. Boundary conditions typically involve specification of

$$u = \hat{u} \quad \text{on } \partial_1\Omega, \qquad \boldsymbol{\sigma}\cdot\mathbf{n} = \hat{\tau} \quad \text{on } \partial_2\Omega, \tag{2.8}$$

where $\partial_1\Omega$ and $\partial_2\Omega$ are complementary subsets of $\partial\Omega$. The *equilibrium problem* with u and $\Gamma_t = \Gamma$ both time independent is studied in [26, 27]. For stability reasons, an additional restriction is imposed: the strains in either phase are confined to neighborhoods of the minima of W (wells), in order to avoid regimes where the W is nonconvex. It is found that the configuration of Γ is severely restricted by this requirement. In particular, the interface normal $\mathbf{n}$ is confined to be close to the direction of the twinning shear vector $\boldsymbol{\xi}$, while the interface itself cannot have corners but may have cusps. The only equilibria with zero energy are such that Γ is a collection of parallel straight lines normal to $\boldsymbol{\xi}$, so that the high- and low-strain regions are parallel layers. The strain alternates from $\nabla u = \mathbf{0}$ to $\nabla u = \boldsymbol{\xi}$ in alternate layers, so that u is piecewise linear. This layered microstructure is observed experimentally [9]. On the other hand, if Γ is a bounded closed curve, then it must have the shape of a *lamella* or flat needle normal to $\boldsymbol{\xi}$ and must terminate in cusps. Similar restrictions on the shape of evolving interfaces arise from preliminary dynamic studies [28, 34] where the needlelike cusped morphology is also found to be possible.

3. REGULARIZATION: THE LEVEL-SET FORMULATION

With a view toward numerical computation, we construct an alternative regularized version of the sharp-interface theory just described. Our approach replaces the interface Γ_t with a smooth transition layer of specified thickness, say ε. Outside this layer the field equations of the sharp-interface model are maintained, while within the layer the stored-energy function W undergoes a smooth transition from the low-strain branch W_0 to the high-strain branch W_1; see (1.5). Special emphasis is placed on the kinetics of the layer. We obtain regularized analogues of the driving traction f and interface velocity and relate them with a kinetic relation formally identical to the one specified in the sharp-interface theory. We try to avoid introducing additional physics through the regularization but instead focus on remaining as faithful to the sharp-interface model as possible.

We introduce a new field, called the *level-set function* $\varphi(\mathbf{x}, t)$, with the property that

$$\varphi > 0 \quad \text{on } \Omega_t^+; \qquad \varphi < 0 \quad \text{on } \Omega_t^-; \qquad \Gamma_t = \{\mathbf{x} \in \Omega : \varphi(\mathbf{x}, t) = 0\} \tag{3.1}$$

so that the interface Γ_t is the zero level set of φ. For example, φ may be chosen as signed distance from Γ_t, namely

$$\varphi(\mathbf{x}, t) = \pm \operatorname{dist}(\Gamma_t, \mathbf{x}), \qquad \mathbf{x} \in \Omega_t^{\pm}. \tag{3.2}$$

The level sets $\varphi = \text{const.}$ are moving curves whose normal velocity $V(\mathbf{x}, t)$ obeys

$$\varphi_t - V|\nabla\varphi| = 0 \qquad \text{on } \Omega. \tag{3.3}$$

Note that this defines V globally on Ω; its values on Γ_t give the interface velocity. The sign of V in (3.3) is chosen so that V is positive when Ω_t^+ grows at the expense of Ω_t^-. We turn next to the regularization of the stored-energy function. For $0 \le h \le 1$, let $\hat{W}(\gamma, h)$ be a smooth function that interpolates between the two branches of the stored-energy function in (1.5), so that

$$\hat{W}(\gamma, 0) = W_0(\gamma), \qquad \hat{W}(\gamma, 1) = W_1(\gamma). \tag{3.4}$$

Let H be the Heaviside step function, with $H(z) = 1$ for $z > 0$ and $H(z) = 0$ for $z < 0$. Recalling (3.1) we can write $\hat{W}(\gamma, H(\varphi))$ for the stored energy of the sharp-interface model, noting that it switches from the low-strain branch W_0 to the high-strain branch W_1 across the interface Γ_t. For each $\varepsilon > 0$ let H_ε be a *regularized Heaviside function*; we require H_ε to be smooth and monotonically nondecreasing with

$$H_\varepsilon'(z) > 0 \quad \text{for } |z| < \varepsilon; \qquad H_\varepsilon(z) = \begin{cases} 0 & \text{for } z < -\varepsilon, \\ 1 & \text{for } z > \varepsilon. \end{cases} \tag{3.5}$$

The regularized Dirac delta function is the derivative

$$\delta_\varepsilon(z) = H_\varepsilon'(z). \tag{3.6}$$

The first step of the regularization procedure is to replace W wherever it occurs with the *regularized stored-energy function*

$$W_\varepsilon(\gamma, \varphi) = \hat{W}(\gamma, H_\varepsilon(\varphi)). \tag{3.7}$$

In effect this replaces the interfacial discontinuity at Γ_t with a *transition layer*

$$\Gamma_t^\varepsilon = \{\mathbf{x} \in \Omega : |\varphi(\mathbf{x}, t)| < \varepsilon\}, \tag{3.8}$$

whose width is approximately 2ε. The *regularized stress* is defined in direct analogy with (1.3):

$$\boldsymbol{\sigma}_\varepsilon(\gamma, \varphi) = \frac{\partial}{\partial \gamma} W_\varepsilon(\gamma, \varphi). \tag{3.9}$$

To illustrate this idea we consider two examples of regularized energies:

Model I. One possibility is a linear interpolation between the low- and high-strain branches W_0 and W_1, so that (3.4) is satisfied:

$$\hat{W}(\gamma, h) = W_0(\gamma) + h[W_1(\gamma) - W_0(\gamma)].$$

In view of (3.7) the regularized stored energy becomes

$$W_\varepsilon(\gamma, \varphi) = W_0(\gamma) + H_\varepsilon(\varphi)[W_1(\gamma) - W_0(\gamma)]. \tag{3.10}$$

Model II. If the low- and high-strain branches W_0 and W_1 are related by a translation, as in the special model (2.1), one may alternatively set $\hat{W}(\gamma, h) = W_0(\gamma - h\boldsymbol{\xi})$, so that in (3.7) we obtain

$$W_\varepsilon(\gamma, \varphi) = W_0(\gamma - H_\varepsilon(\varphi)\boldsymbol{\xi}). \tag{3.11}$$

Similar constructions were employed by Fried and Gurtin [13].

Next, we enforce the global forms of momentum balance (1.2) and the dissipation inequality (1.10), but with W and $\boldsymbol{\sigma}$ replaced with their regularized counterparts W_ε and $\boldsymbol{\sigma}_\varepsilon$. Momentum balance reduces to the local equation of motion (1.8) in terms of $\boldsymbol{\sigma}_\varepsilon$:

$$\nabla \cdot \boldsymbol{\sigma}_\varepsilon(\nabla u, \varphi) = \rho u_{tt} \qquad \text{on } \Omega. \tag{3.12}$$

A simple calculation utilizing (3.7), (3.8), (3.12) and the divergence theorem shows that the analogue of the dissipation rate in (1.10) satisfies

$$\Delta_\varepsilon(t) = \int_{\partial\Omega} u_t \boldsymbol{\sigma}_\varepsilon \cdot \mathbf{n}\, ds - \frac{d}{dt}\int_\Omega \left(W_\varepsilon + \frac{1}{2}\rho u_t^2\right) dA = -\int_\Omega \frac{\partial W_\varepsilon}{\partial \varphi}\varphi_t\, dA. \tag{3.13}$$

If we now define the *regularized driving traction* as

$$f_\varepsilon = -\frac{\partial \hat{W}}{\partial h}(\gamma, H_\varepsilon(\varphi)) \tag{3.14}$$

and employ (3.3), (3.6), and (3.7), we conclude from (3.13) that

$$\Delta_\varepsilon(t) = \int_\Omega f_\varepsilon V \delta_\varepsilon(\varphi)|\nabla\varphi|\, dA. \tag{3.15}$$

The normal velocity V of level sets enters this expression after use of (3.3). Note that $\delta_\varepsilon(\varphi)$—hence the integrand in (3.15)—vanishes outside the transition layer Γ_t^ε in view of (3.6), (3.8). The regularized driving traction f_ε is a globally defined field, whereas f in the sharp-interface theory is only defined on the interface Γ_t. Its definition (3.14) is motivated by a comparison of (3.15) with (1.11). Indeed, if φ vanishes on Γ_t and θ is any smooth field, one can adopt an argument of Chang *et al.* [8] to show that

$$\int_\Omega \theta\delta(\varphi)|\nabla\varphi|\,dA = \int_{\Gamma_t} \theta\,ds$$

in terms of the Dirac delta distribution. This shows that (3.15) is a regularized analogue of (1.11).

It remains to determine the evolution of the interface Γ_t. Here we adopt the kinetic relation of the sharp-interface theory (1.14). Note that the unit normal vector to level sets of φ—such as Γ_t—is given by

$$\mathbf{n} = \frac{\nabla\varphi}{|\nabla\varphi|} \qquad \text{on } \Omega. \tag{3.16}$$

The kinetic relation is enforced in terms of the regularized driving traction of (3.14) in a fashion formally identical to (1.14):

$$V = g\left(f_\varepsilon, \frac{\nabla\varphi}{|\nabla\varphi|}\right).$$

Substituting this for V into (3.3) yields an evolution equation for the level-set function φ, after observing that f_ε in (3.14) and V are now fields defined throughout Ω:

$$\varphi_t - g\left(f_\varepsilon, \frac{\nabla\varphi}{|\nabla\varphi|}\right)|\nabla\varphi| = 0 \qquad \text{on } \Omega. \tag{3.17}$$

Equations (3.12) and (3.17) comprise a system of two coupled partial differential equations for u and φ. Given the regularized stored-energy function W_ε in (3.7) and the kinetic relation g in (1.14), one determines $\boldsymbol{\sigma}_\varepsilon$ and f_ε from (3.9) and (3.14), respectively. The *regularized problem* consists of solving (3.12) and (3.17) for the two unknown functions u and φ, subject to the initial conditions

$$u(\mathbf{x}, 0) = u_0(\mathbf{x}), \quad u_t(\mathbf{x}, 0) = v_0(\mathbf{x}), \quad \varphi(\mathbf{x}, 0) = \varphi_0(\mathbf{x}) \qquad \text{for } \mathbf{x} \in \Omega, \tag{3.18}$$

and the boundary condition

$$u = \hat{u} \qquad \text{on } \partial\Omega. \tag{3.19}$$

We choose φ_0 as signed distance from the initial interface Γ_0. For simplicity we only consider Dirichlet boundary conditions for u. The issue of boundary conditions for φ is considered in Section 5. A substantial advantage of the above construction is the elimination of all jump conditions by the regularization procedure. Once the regularized problem is solved, the evolving interface Γ_t is easily determined as the zero-level set of $\varphi(\mathbf{x}, t)$; see (3.1).

4. THE REGULARIZED PROBLEM FOR A SPECIAL MODEL

We restrict attention to the special constitutive law (2.1) and the kinetic relation (2.6). For Model I, the regularized stored energy (3.10) now takes the form

$$W_\varepsilon(\gamma, \varphi) = \frac{\mu}{2}\big[|\gamma|^2 + H_\varepsilon(\varphi)(|\boldsymbol{\xi}|^2 - 2\boldsymbol{\xi}\cdot\gamma)\big]. \tag{4.1}$$

For the alternative Model II, (3.11) yields

$$W_\varepsilon(\gamma, \varphi) = \frac{\mu}{2}|\gamma - H_\varepsilon(\varphi)\boldsymbol{\xi}|^2. \tag{4.2}$$

The regularized stress (3.9) is the same for both models:

$$\boldsymbol{\sigma}_\varepsilon(\gamma, \varphi) = \mu[\gamma - H_\varepsilon(\varphi)\boldsymbol{\xi}]. \tag{4.3}$$

On the other hand, (3.14) in conjunction with (4.1), (4.2) results in different versions of the regularized driving traction:

$$\begin{aligned} &\text{Model I:} \qquad f_\varepsilon(\gamma, \varphi) = \mu\boldsymbol{\xi}\cdot\left(\gamma - \frac{1}{2}\boldsymbol{\xi}\right),\\ &\text{Model II:} \qquad f_\varepsilon(\gamma, \varphi) = \mu\boldsymbol{\xi}\cdot(\gamma - H_\varepsilon(\varphi)\boldsymbol{\xi}). \end{aligned} \tag{4.4}$$

Observe that the values of the two versions of f_ε agree on the interface Γ_t, where $\varphi = 0$. Noting that $H_\varepsilon(0) = 1/2$ and using (2.2), we find for both models

$$f_\varepsilon(\gamma, 0) = \frac{1}{2}\boldsymbol{\xi}\cdot[\boldsymbol{\sigma}^1(\gamma) + \boldsymbol{\sigma}^0(\gamma)]. \tag{4.5}$$

Compare this with (2.5). In both the sharp-inerface theory and the regularized model, the driving traction at the interface is proportional to the average of the stresses corresponding to the two phases. Choosing the coordinate system so that $\boldsymbol{\xi} = (0, \xi)$, let $\mathbf{x} = (x, y)$, $\mathbf{n} = (n_1, n_2)$. We consider a slight generalization of the kinetic relation (2.6), namely, a combination of an isotropic relation $V = M_1 f$ and the anisotropic version (2.6). The linear dependence on f is chosen for simplicity. Given two constants $M_i \geq 0$, we set

$$V = g(f, \mathbf{n}) = M_1 f + M_2|n_1| f. \tag{4.6}$$

Substitution of (4.3) into (3.12) furnishes the momentum-balance equation:

$$\Delta u - \frac{1}{c^2}u_{tt} = \xi\delta_\varepsilon(\varphi)\varphi_y \qquad \text{on } \Omega. \tag{4.7}$$

In the evolution equation (3.17) for φ, we employ the kinetic relation (4.6) with f and $\mathbf{n}$ replaced with their regular counterparts (4.4) and (3.16), respectively. The special version of the evolution equation (3.17) so obtained reads

$$\text{Model I:} \qquad \varphi_t - \xi\mu(u_y - \xi/2)(M_1|\nabla\varphi| + M_2|\varphi_x|) = 0 \tag{4.8}$$

and alternatively

$$\text{Model II:} \qquad \varphi_t - \xi\mu(u_y - \xi H_\varepsilon(\varphi))(M_1|\nabla\varphi| + M_2|\varphi_x|) = 0. \tag{4.9}$$

We impose the Dirichlet boundary condition

$$u = ky \qquad \text{on } \partial\Omega, \tag{4.10}$$

where the constant $0 \le k \le \xi/2$ is the *applied shear*. The explicit appearance of the constitutive parameters μ, c, and ξ may be avoided by introducing the change of variables

$$\hat{t} = ct, \qquad \hat{u}(x, y, \hat{t}) = \frac{1}{\xi}(u(x, y, \hat{t}/c) - ky), \qquad \hat{\varphi}(x, y, \hat{t}) = \varphi(x, y, \hat{t}/c). \quad (4.11)$$

Note that $\hat{u}$ satisfies $\hat{u} = 0$ on $\partial\Omega$. Define the normalized parameters

$$\hat{k} = k/\xi, \qquad \hat{M}_i = \xi^2 \mu M_i/c. \quad (4.12)$$

In terms of these new variables (after dropping hat overscripts) we obtain normalized versions of Eqs. (4.7) and (4.8) for Model I:

$$\Delta u - u_{tt} = \delta_\varepsilon(\varphi)\varphi_y \qquad \text{on } \Omega \quad (4.13)$$

and

$$\varphi_t - (u_y + k - 1/2)(M_1|\nabla\varphi| + M_2|\varphi_x|) = 0 \qquad \text{on } \Omega. \quad (4.14)$$

The system consisting of (4.13) and (4.14) is to be studied numerically according to a procedure laid out in the rest of the paper.

5. FINITE-DIFFERENCE DISCRETIZATION

We describe finite-difference discretizations for the regularized model (level-set formulation) developed in the previous section. First, we specify regularized versions of the singular Dirac delta function δ and the discontinuous Heaviside function H. As in [8], we define the regularized delta function δ_ε as

$$\delta_\varepsilon(z) = \begin{cases} \frac{1}{2}(1 + \cos(\pi z/\varepsilon))/\varepsilon & \text{for } |z| < \varepsilon, \\ 0 & \text{for } |z| \ge \varepsilon, \end{cases}$$

and a corresponding regularized Heaviside function H_ε as

$$H_\varepsilon(z) = \begin{cases} 0 & \text{for } z < -\varepsilon \\ (z + \varepsilon)/(2\varepsilon) + \sin(\pi z/\varepsilon)/(2\pi) & \text{for } |z| \le \varepsilon, \\ 1 & \text{for } z > \varepsilon, \end{cases}$$

so that the relation $H'_\varepsilon(x) = \delta_\varepsilon(x)$ holds.

An $N \times N$ grid (with spacing $h = 1/N$) is laid on Ω. Denote by $u^n_{i,j}$ the approximation of $u(x_i, y_j, t_n)$, where $x_i = ih$, $y_j = jh$, $t_n = n\Delta t$, and Δt is the time step; here $i, j = 1, \ldots, N$, while n is a nonnegative integer. $\varphi^n_{i,j}$ is defined similarly. Here $i, j = 1, \ldots, N$, while n is a nonnegative integer. We use a second-order, centered-difference discretization in space and time for the normalized momentum-balance equation (4.13). Introduce the difference operators

$$D^x_0 f_{i,j} = (f_{i+1,j} - f_{i-1,j})/2h \qquad \text{(centered)},$$
$$D^x_- f_{i,j} = (f_{i,j} - f_{i-1,j})/h \qquad \text{(backward)},$$
$$D^x_+ f_{i,j} = (f_{i+1,j} - f_{i,j})/h \qquad \text{(forward)}.$$

The operators D_0^y, D_-^y, and D_+^y are defined similarly. The centered-difference approximation to the Laplacian operator Δ then takes the form $\Delta_h = D_-^x D_+^x + D_-^y D_+^y$. The discretized version of (4.13) thus reads $D_-^t D_+^t u_{i,j}^n = \Delta_h u_{i,j}^n - \delta_\varepsilon(\varphi_{i,j}^n) D_0^y u_{i,j}^n$, or more specifically,

$$\frac{u_{i,j}^{n+1} - 2u_{i,j}^n + u_{i,j}^{n-1}}{\Delta t^2} = \frac{u_{i+1,j}^n + u_{i-1,j}^n - 4u_{i,j}^n + u_{i,j+1}^n + u_{i,j-1}^n}{h^2} - \delta_\varepsilon\big(\varphi_{i,j}^n\big)\frac{\varphi_{i,j+1}^n - \varphi_{i,j-1}^n}{2h}.$$

On the other hand, we employ a second-order ENO scheme to discretize Eq. (4.14) describing the evolution of the level-set function φ. Since we are interested in accurately computing the convection of interface position, we use the nonconservative form of the ENO scheme [8]. Define a minmod function as

$$\operatorname{minmod}(u, v) = \begin{cases} \operatorname{sgn}(u)\min(|u|, |v|) & \text{if } uv > 0, \\ 0 & \text{otherwise.} \end{cases}$$

Here sgn stands for the signum function. Equation (4.14) satisfied by the level-set function φ is a specialized version of the Hamilton–Jacobi equation $\varphi_t - V|\nabla\varphi| = 0$ (see (3.3), (3.17), (4.6)). Suppose momentarily that the normal velocity $V = V(\mathbf{x}, t)$ of the level sets of φ is known. The second-order ENO discretization of the Hamilton–Jacobi equation is given by

$$\varphi_{i,j}^{n+1} = \begin{cases} \varphi_{i,j}^n - \Delta t V_{i,j}^n P_+ & \text{for } V_{i,j}^n > 0, \\ \varphi_{i,j}^n - \Delta t V_{i,j}^n P_- & \text{for } V_{i,j}^n \le 0, \end{cases}$$

where

$$\begin{aligned}
P_+ &= \sqrt{(\max(p_-^x, 0)^2 + \min(p_+^x, 0)^2) + (\max(p_-^y, 0)^2 + \min(p_+^y, 0)^2)}, \\
P_- &= \sqrt{(\min(p_-^x, 0)^2 + \max(p_+^x, 0)^2) + (\min(p_-^y, 0)^2 + \max(p_+^y, 0)^2)}, \\
p_-^x &= D_-^x \varphi_{i,j}^n + 0.5h \operatorname{minmod}\big(D_-^x D_+^x \varphi_{i,j}^n,\, D_-^x D_+^x \varphi_{i-1,j}^n\big), \\
p_+^x &= D_-^x \varphi_{i+1,j}^n - 0.5h \operatorname{minmod}\big(D_-^x D_+^x \varphi_{i+1,j}^n,\, D_-^x D_+^x \varphi_{i,j}^n\big), \\
p_-^y &= D_-^y \varphi_{i,j}^n + 0.5h \operatorname{minmod}\big(D_-^y D_+^y \varphi_{i,j}^n,\, D_-^y D_+^y \varphi_{i,j-1}^n\big), \\
p_+^y &= D_-^y \varphi_{i,j+1}^n - 0.5h \operatorname{minmod}\big(D_-^y D_+^y \varphi_{i,j+1}^n,\, D_-^y D_+^y \varphi_{i,j}^n\big).
\end{aligned}$$

The specific version of (4.14) also involves a term $V|\varphi_x|$, whose second-order ENO discretization is obtained by removing the terms corresponding to φ_y above.

Reinitialization and Boundary Conditions for the Level-Set Function

In general, even if we prescribe the initial value of the level-set function φ to equal signed distance from the interface, it will not remain a distance function at later times. For large-time computations it is desirable to keep φ as a distance function. This will ensure that the interface has a finite thickness of order ε for all time. In [30], an iterative procedure was proposed to *reinitialize* φ at each time step, so that it remains a signed distance function from the evolving interface. Specifically, given a level-set function $\varphi_*(\mathbf{x}) = \varphi(\mathbf{x}, t_*)$ at a fixed time t_*, one computes the solution of the initial-value problem

$$\begin{aligned}
\varphi_t &= \operatorname{sgn}(\varphi_*)(1 - |\nabla\varphi|), \\
\varphi(\mathbf{x}, 0) &= \varphi_*(\mathbf{x}) \qquad \text{on } \Omega.
\end{aligned} \tag{5.1}$$

The solution converges rapidly in time to a function that has the same sign and the same zero level set as φ_*, and also satisfies $|\nabla\varphi| = 1$, so that it equals signed distance from the interface. After φ evolves at each time step according to (4.14), it is reinitialized by solving (5.1) for two time steps; this suffices due to rapid convergence. This procedure is crucial for our formulation, since the extension of the normal velocity V in our case is not continuous across the phase boundary in the sharp-interface ($\varepsilon \to 0$) limit. This makes computations more difficult than in the fluid interface problem considered in [8, 30], where the normal velocity is continuous across the interface.

We consider next the issue of boundary conditions for the level-set function at the boundary $\partial\Omega$. In our calculations we use a one-sided difference approximation for φ_x and φ_y at the boundary. For example, at the sides $x = 0, 1$ we approximate $\varphi_x(0, y_j, t_n)$ by $D^x_+\varphi^n_{0,j} = (\varphi^n_{1,j} - \varphi^n_{0,j})/h$ and $\varphi_x(1, y_j, t_n)$ by $D^x_-\varphi^n_{N,j} = (\varphi^n_{N,j} - \varphi^n_{N-1,j})/h$.

When the normal velocity V is nonnegative (the interface moves toward $\partial\Omega$), this provides an upwind approximation of the Hamilton–Jacobi equation and results in a stable discretization. However, we find in our computations that the interface splits at the boundary and comes back into the domain, so that the normal velocity becomes negative over certain interface portions. Then the one-sided boundary condition we use is a downwind approximation and causes numerical instability. It is our reinitialization process that stabilizes the scheme. On the other hand, one must provide some artificial boundary condition for φ in order to continue the computation after the interface splits. One should note that the level-set function is physically relevant only to the extent that it describes the interface position, where $\varphi = 0$. Hence, the manner in which we specify boundary conditions for φ does not change the physics of the problem, as long as the interface does not intersect the domain boundary. In the problem examined here, the high-strain zone bounded by the interface is prohibited from extending to the boundary because of the boundary conditions for u, which force the neighborhood of the boundary portions $x = 0, 1$ to be in the low-strain phase. Instead, the interface may taper into tips that touch $\partial\Omega$ only at a finite number of points. The interface still satisfies the evolution equations in the interior and the boundary condition for the displacement u is strictly enforced. In some sense, our specific numerical boundary condition and the reinitialization process provide a way to continue the interface solution after it reaches the domain boundary. The interface chooses to split afterward so that it can further decrease the total energy. This splitting is observed in experiments (9) and is consistent with our understanding that solutions that tend to minimize energy develop fine-scale structures in time.

We only employ Model I in our computations. An additional numerical difficulty arises in computations with Model II. In particular, the normal velocity of the interface in (4.9) (Model II) involves the difference of two functions $u_y - \xi H_\varepsilon(\varphi)$. In the sharp-interface theory, both terms represent discontinuous functions across the interface. In the sharp-interface ($\varepsilon \to 0$) limit, the second term involves a step function, while the discontinuity in u_y is due to the Dirac delta term in the wave equation (4.13) when $\varepsilon \to 0$, or equivalently, to the jump conditions (2.4). In the regularized model, however, the discretized versions of u_y and $H_\varepsilon(\varphi)$ may have different structures in the interface layer. In the numerical calculations, these differences can produce overshoot and undershoot across the interface. This can lead to order $O(1)$ errors in interface velocity. On the other hand, the corresponding term in (4.8) (Model I) reads $u_y - \xi/2$ and involves only one discontinuous term u_y. One can show that the behavior of the term u_y in Model I tends to sharpen the interface layer by locally increasing $|\nabla\varphi|$. This tends to improve the determination of the interface position. The reinitialization

scheme for φ discussed above serves to maintain the layer thickness to be of order ε for all time. In Model II, however, the interplay of u_y and $H_\varepsilon(\varphi)$ may tend to flatten the level-set function at the interface, thereby increasing uncertainty in interface position. Consequently, Model I is preferable from the computational standpoint and is used throughout.

6. NUMERICAL RESULTS

The problem we consider is the dynamic evolution of a *twin nucleus*, that is, a small region in the high-strain phase that is assumed to have already nucleated at the center of the unit square $\Omega = (0, 1) \times (0, 1)$, subject to displacement boundary conditions corresponding to constant applied shear loading. Specifically we impose the Dirichlet boundary condition $u = ky$ on $\partial\Omega$, where the constant $0 \le k \le \xi/2$ is the *applied shear*. In the remainder of the paper, all quantities stand for their normalized counterparts, defined in (4.11) and (4.12). The boundary condition reduces to

$$u = 0 \qquad \text{on } \partial\Omega. \tag{6.1}$$

For convenience, the initial interface (nucleus boundary) Γ_0 is chosen to be an ellipse centered at (0.5, 0) with semimajor axis $a = 0.3$ and semiminor axis $b = 0.15$. The initial value φ_0 of the level-set function in (3.18) is set to signed distance from Γ_0 (positive inside Γ_0). We also let initial velocity $v_0 = 0$ and choose the initial displacement u_0 as the *elastic equilibrium* (time-independent) solution of the momentum-balance equation (4.13), namely

$$\Delta u_0 = \delta_\varepsilon(\varphi_0)\frac{\partial \varphi_0}{\partial y} \quad \text{on } \Omega; \qquad u_0 = 0 \quad \text{on } \partial\Omega. \tag{6.2}$$

The initial displacement u_0 is plotted in Fig. 1. Observe that it is almost linear inside the initial ellipse. This is in agreement with a standard result from potential theory that applies to the sharp-interface version of problem (6.2); see [26].

It turns out that the initial driving traction (4.5) does not vanish. The kinetic relation (4.6) forces the interface to move; equivalently, the level-set function φ changes as dictated by (4.14). The coupling of u and φ in (4.13) and (4.14) drives the subsequent dynamics of the problem.

All calculations were performed with $N = 256$, $\varepsilon = 0.01$. We compare various choices of the mobility coefficients M_1, M_2 in the kinetic relation (4.6). An isotropic kinetic relation would have $M_1 > 0$, $M_2 = 0$ in (4.6) and (4.14). This seems unreasonable for the anisotropic twinning problem. The fully anisotropic kinetic relation with $M_1 = 0$, $M_2 > 0$ can be motivated from a micromechanical model that views the interface as a collection of twinning dislocations [34]. These dislocations can glide on twinning planes (move along the x direction), but cannot climb (move along the y direction). Thus this kinetic relation allows motion of the interface in the x direction, but inhibits motion in the y direction. We compare this with isotropic kinetics ($M_1 = 1$, $M_2 = 0$), but also consider a version that combines a small isotropic term with the anisotropic one ($M_1 = 0.1$, $M_2 = 3$). We also consider different levels of loading, controlled by the applied shear k.

Cusp Formation

Our first calculation studies initial interfacial shape evolution for short times $t = 0$ to $t = 1$. We choose $k = 0.3$, $M_1 = 0$, $M_2 = 3$ (fully anisotropic kinetics) and $a = 0.3$, $b = 0.15$. In Fig. 2, we plot a sequence of evolving configurations of the interface at $t = 0, 0.2, 0.5, 1$.

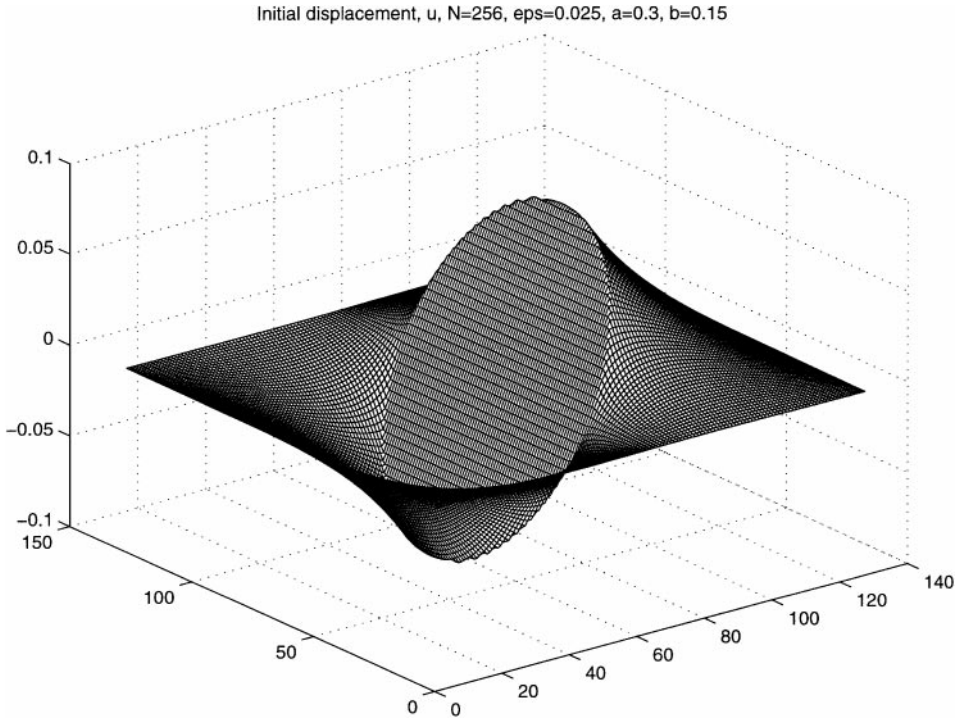

FIG. 1. The initial displacement u_0 (solution of (6.2)) for an initial ellipse with $a = 0.3$, $b = 0.15$, $N = 256$, $\varepsilon = 0.01$.

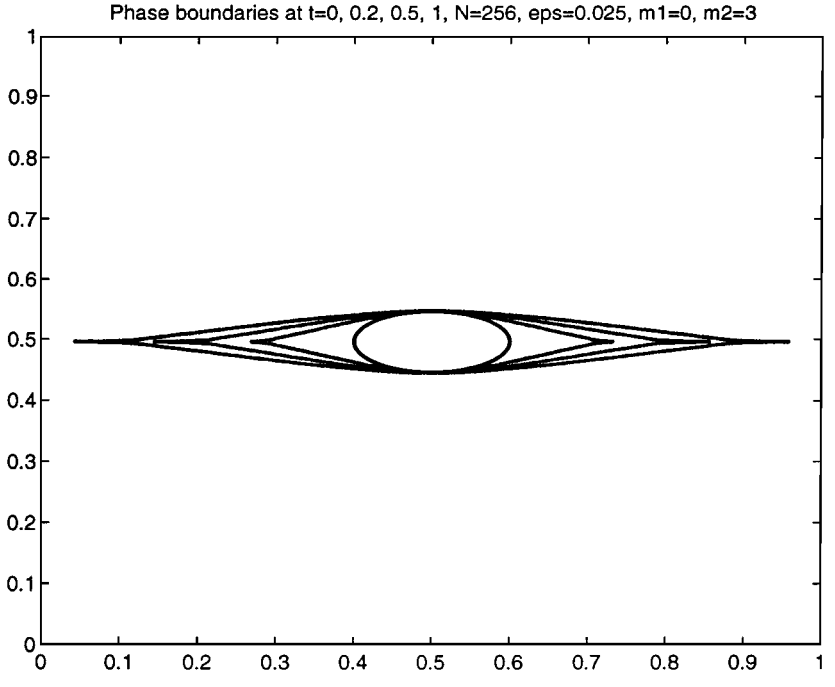

FIG. 2. A sequence of evolving interface configurations at $t = 0, 0.2, 0.5, 1$ for fully anisotropic kinetics with $M_1 = 0$, $M_2 = 3$. Here $a = 0.3$, $b = 0.15$, $k = 0.3$.

The interface grows mainly in the horizontal direction from the initial smooth ellipse. It quickly develops two sharp tips, which have the appearance of *cusps* and propagate toward the boundary. The high-strain region develops a *lamellar*, needlelike form that tapers into cusped tips. This generic form is deduced in analytical solutions of both static [26, 27] and dynamic [28, 29] versions of the sharp-interface twinning problem. Experimentally observed twin boundaries are commonly in the form of elongated cusped needles along specific directions [9]. During growth, the tips are observed to propagate by motion along the axis of the needle.

Effect of Kinetic Anisotropy

We compare the effect of isotropic versus anisotropic kinetics in Figs. 3a and 3b, respectively. In both cases we impose the same initial conditions with $a = 0.2$, $b = 0.1$, $k = 0.3$. For the isotropic case we set $M_1 = 1$, $M_2 = 0$. The growing tips in Fig. 3a remain rounded and do not assume a cusplike form. In contrast, in Fig. 3b, where a fully anisotropic kinetic relation is chosen with $M_1 = 0$, $M_2 = 1$, the tips immediately become cusped and maintain their sharpness up to contact with the boundary. We regard this as evidence that kinetic anisotropy is essential for the appropriate description of interfacial evolution. Insofar as we know, the rounded-tip form associated with the isotropic case never seems to be experimentally observed.

The effect of the loading level (amount of shear k) for anisotropic kinetics ($M_1 = 0$, $M_2 = 1$) on subsequent interface evolution was studied for $k = 0.2$, 0.3, and 0.4. Results are shown in Figs. 4, 5, and 6, respectively. In all these cases, we observed that once the tip reaches the boundary $\partial\Omega$, it becomes blunted and the cusp develops into a wedge shape. For low loading, $k = 0.2$, the tips remain on the boundary (Fig. 4) up to the end of the calculation.

Tip Splitting

For higher loading ($k = 0.3$, Fig. 5), a *tip splitting* phenomenon occurs between $t = 1$ and $t = 2$. In particular, each tip splits suddenly into two tips that remain on the boundary, and one *reentrant tip* that propagates backward toward the center of the region. At this load level the reentrant tips slow down substantially by $t = 8$. Tip splitting at obstacles is observed experimentally in a Cu–Al–Ni single crystal by Chu and James [9]. It is recognized as a mechanism of lowering the total energy by dividing each needle into thinner, flatter needles. Models focusing on statics of branched twin microstructures may be found in [19, 20].

For even higher loads ($k = 0.4$, $t = 0.5, 1, \ldots, 8$, Fig. 6), multiple splitting events are observed. The first splitting takes place between $t = 0.5$ and $t = 1$. The onset of the second splitting can be seen at $t = 1.5$, and it is more evident by $t = 2$. The third splitting occurs around $t = 3$. There are five reentrant tips on each side that split the original lamella into six branches; the reentrant tips continue to grow throughout the calculation. However, the growth becomes quite slow by $t = 4$. We plot the total kinetic plus elastic energy in Fig. 7. Use of (4.1) and the change of variables (4.11) yields the following expression for the total energy (normalized after division by $\mu\xi^2$):

$$E(t) = \frac{1}{2}\int_0^1 \int_0^1 \left\{u_t^2 + u_x^2 + [u_y + k - H_\varepsilon(\varphi)]^2 + H_\varepsilon(\varphi)[1 - H_\varepsilon(\varphi)]\right\} dx\, dy. \quad (6.3)$$

Since $u_t = 0$ on the boundary in view of boundary condition (4.10), the first integral in

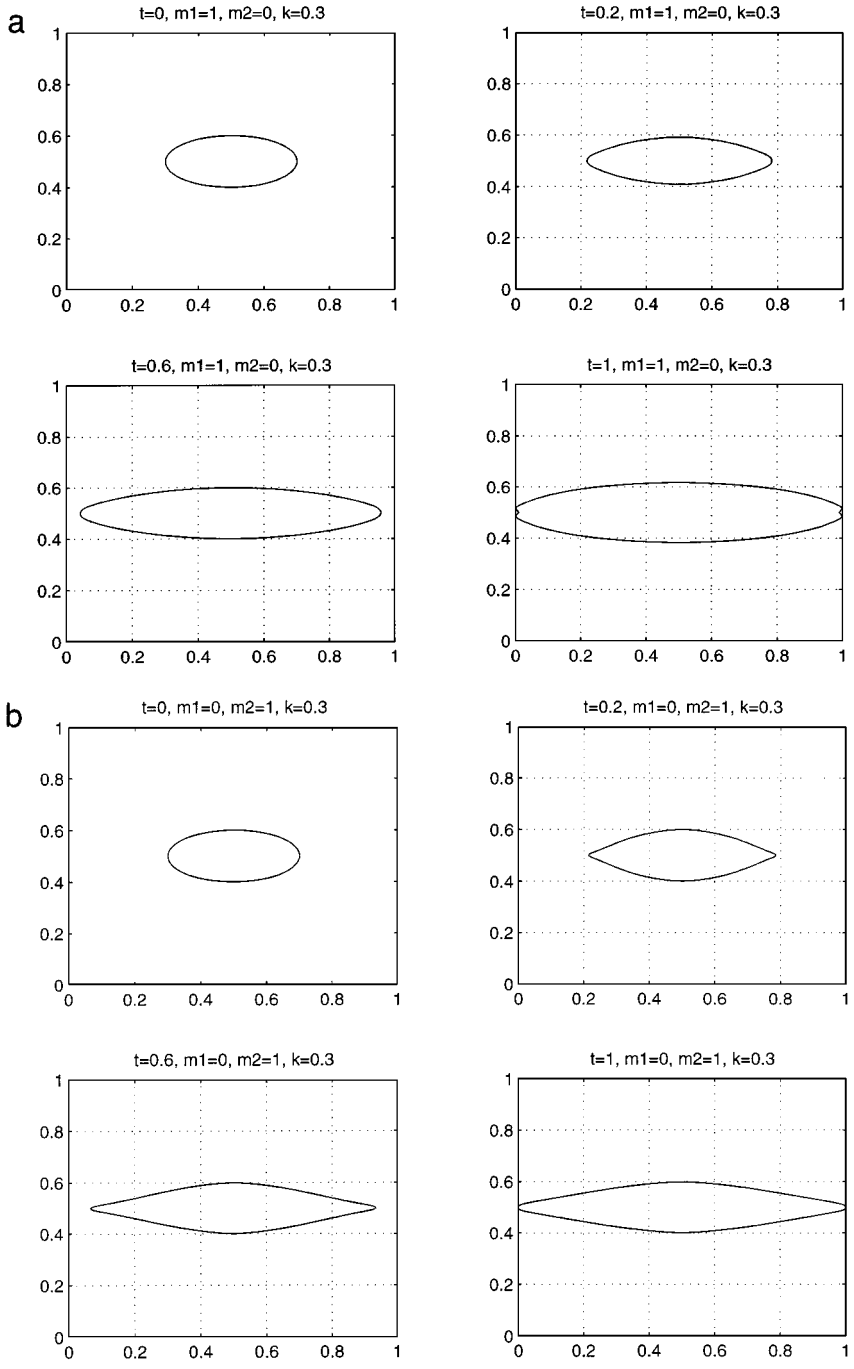

FIG. 3. Comparison of isotropic versus anisotropic kinetics. Sequence of interface configurations at $t = 0, 0.2, 0.6, 1$ for (a) isotropic kinetics with $M_1 = 1$, $M_2 = 0$, $a = 0.2$, $b = 0.1$, $k = 0.3$ and (b) fully anisotropic kinetics with $M_1 = 0$, $M_2 = 1$, $a = 0.2$, $b = 0.1$, $k = 0.3$.

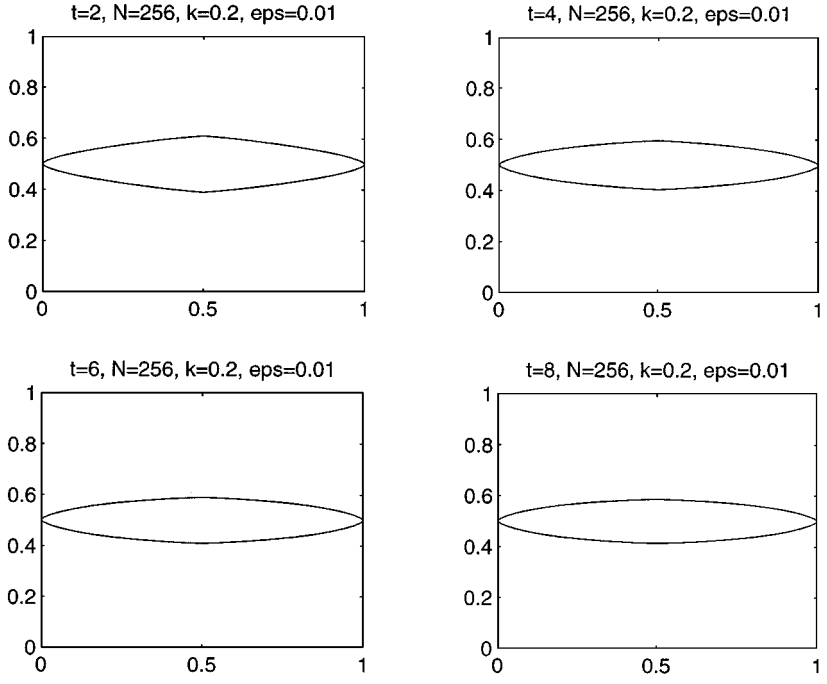

FIG. 4. Sequence of interface configurations at $t = 2, 4, 6, 8$ for low load, $k = 0.2$, and fully anisotropic kinetics; $M_1 = 0$, $M_2 = 1$, $a = 0.3$, $b = 0.15$.

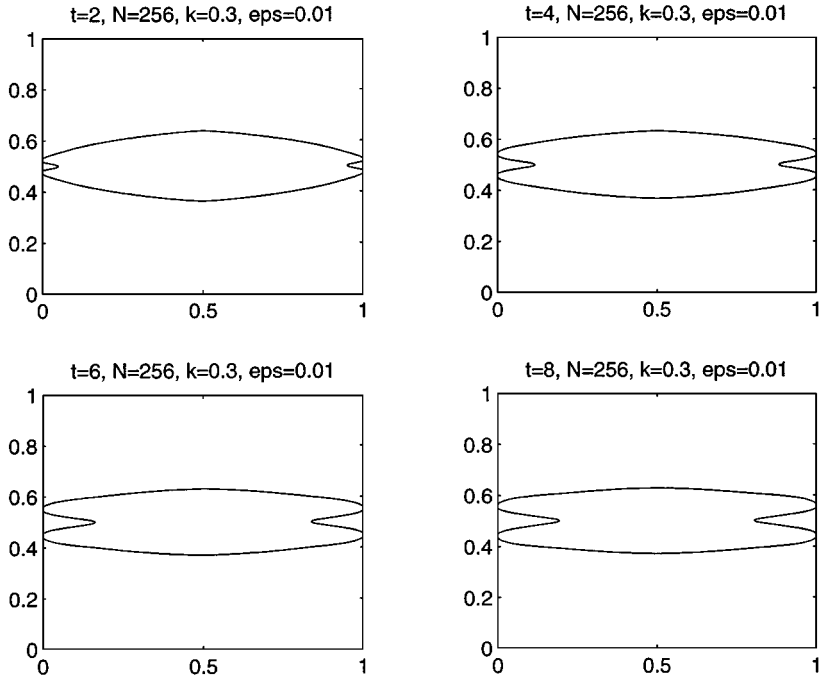

FIG. 5. Sequence of interface configurations at $t = 2, 4, 6, 8$ for intermediate load, $k = 0.3$, and fully anisotropic kinetics; $M_1 = 0$, $M_2 = 1$, $a = 0.3$, $b = 0.15$. Tip splitting has already occurred at $t = 2$.

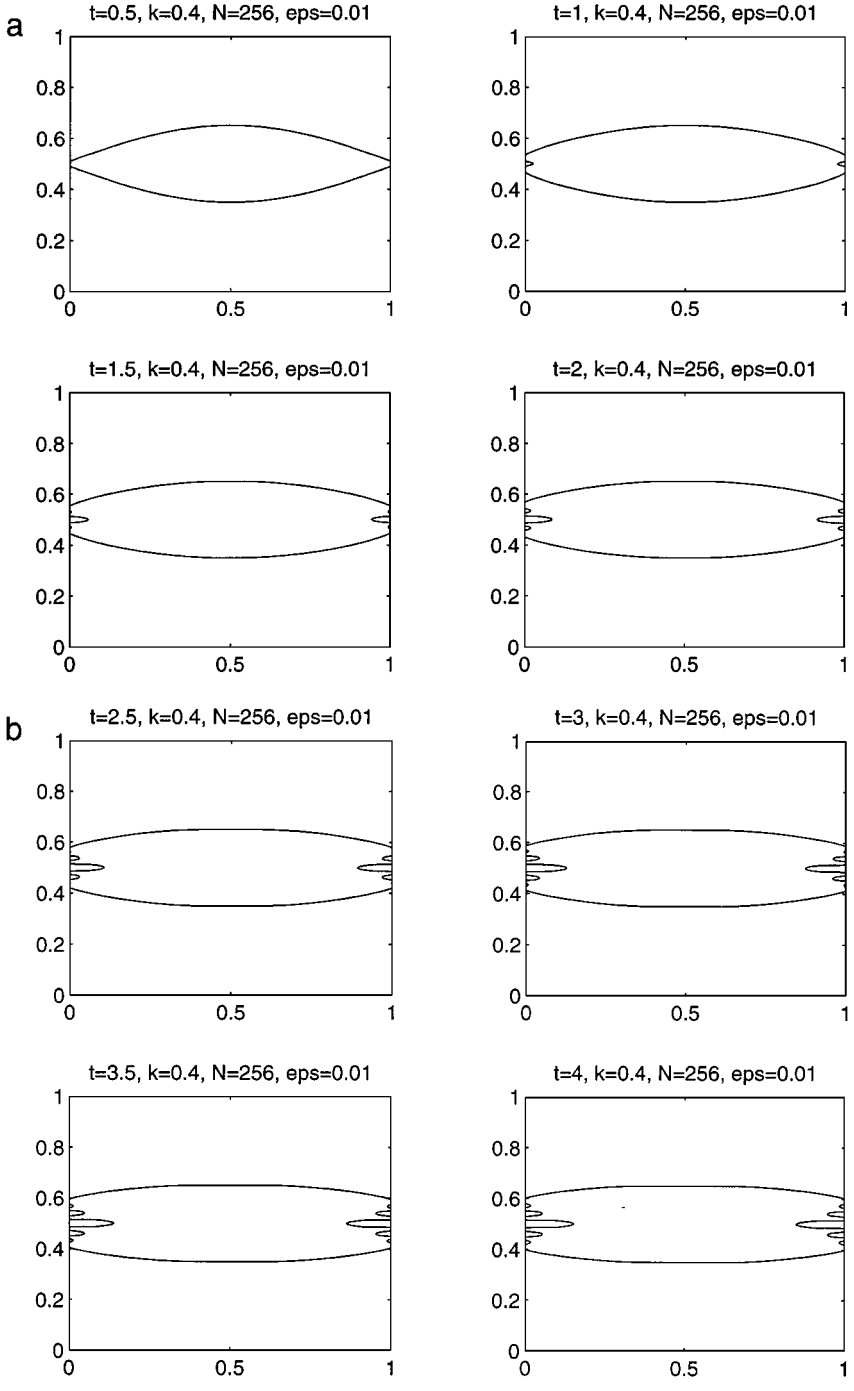

FIG. 6. (a) Sequence of interface configurations at $t = 0.5, 1, 1.5, 2$ for high load, $k = 0.4$, and fully anisotropic kinetics; $M_1 = 0$, $M_2 = 1$, $a = 0.3$, $b = 0.15$. Observe the multiple splittings. (b) Subsequent evolution at $t = 2.5, 3, 3.5, 4$. Parameters are as in (a). (c) Subsequent evolution at $t = 6.5, 7, 7.5, 8$. Parameters are as in (a).

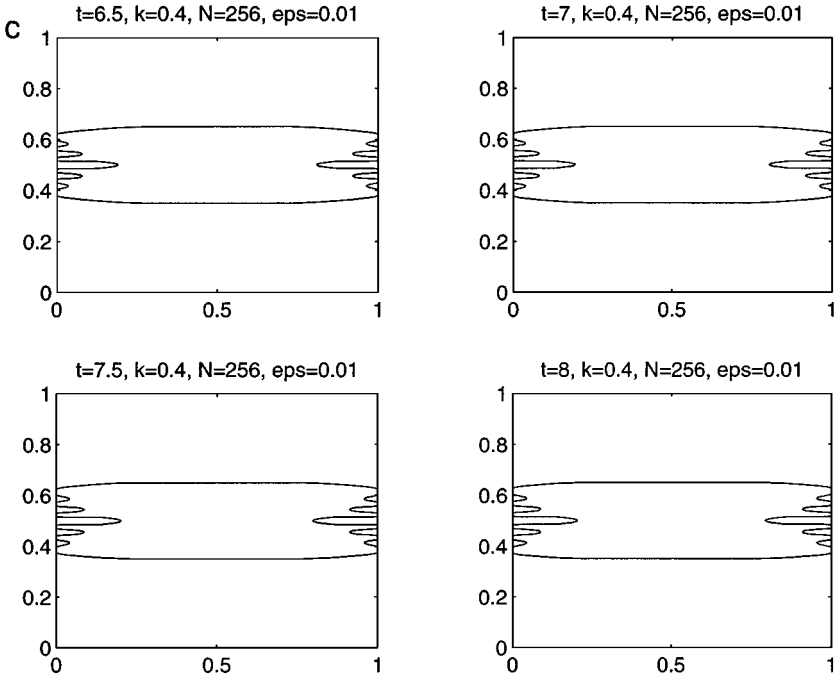

FIG. 6—*Continued*

(1.10) vanishes; as a result the total energy should decrease due to dissipation caused by interface motion. This is confirmed in Fig. 7. The energy decays very slowly after $t = 4$. It is possible that the solution settles down to a local energy minimum without producing more fine structures at the interface and possibly without complete separation, although this is far from certain. Micrographs of twinned microstructures in Cu–Al–Ni [9] show partially split lamellae with two or three tips; complete separation of layers into two or more thinner needles by means of tip splitting also occurred in those experiments. Our model is not intended to capture the complicated behavior of this alloy, nonetheless, the qualitative agreement is quite interesting.

We plot the position of the leading tip as a function of time in Fig. 8. Before the original leading tip reaches the boundary, its speed seems to be almost constant in time. Tip speed has a monotonically increasing dependence on the load level, as expected from the kinetic relation; it varies between about one-fifth of the shear wave speed c for $k = 0.2$ and about one-half for $k = 0.4$. These values seem quite high; they can be reduced by an order of magnitude by setting $M_2 = 0.1$. We note, however, that tip speeds close to $0.4c$ have been reported in experiments by Williams and Reid [36].

For low loading, the tip decelerates at some distance away from the boundary due to interaction with it. Faster tips during high loading maintain their speed almost up to contact with the boundary. The tip stops at the physical boundary and stays there for some time. During this period, the angle of the tip broadens and it becomes somewhat blunted. After a certain time, the tip splits and propagates inward into the domain. The speed of propagation of the reentrant tip is no longer uniform after the interface splits. The speed fluctuations observed in Fig. 8 are due to interaction of the interface with elastic shear waves. The latter are generated during initial interface growth and undergo multiple reflections from the boundary. In particular, the sudden initial motion of the interface causes elastic shear

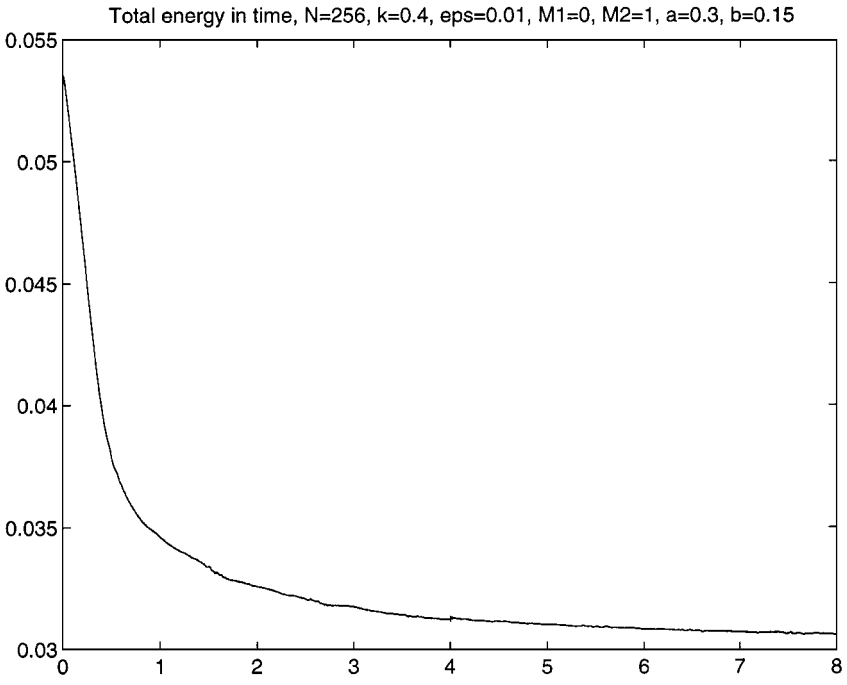

FIG. 7. Total energy versus time for the simulation of Fig. 6 ($k = 0.4$, $M_1 = 0$, $M_2 = 1$, $a = 0.3$, $b = 0.15$).

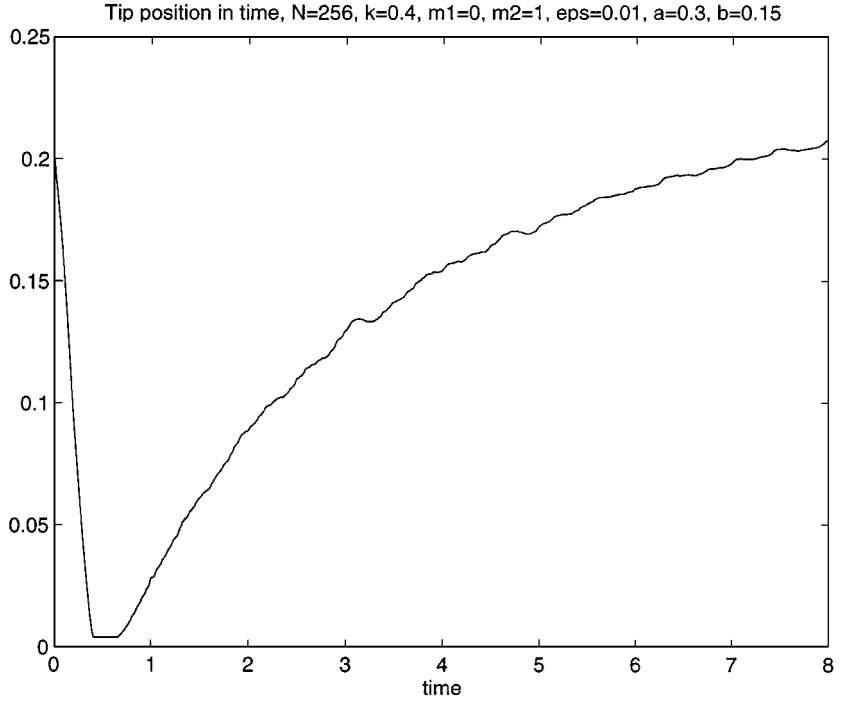

FIG. 8. Position (x-coordinate) versus time of the left leading tip for the simulation of Fig. 6 ($k = 0.4$, $M_1 = 0$, $M_2 = 1$, $a = 0.3$, $b = 0.15$).

waves to emanate from it [3]. Conversely, a shear wave impinging on the interface affects the speed of the latter by altering the local stress state and hence the driving traction.

Topological Changes

In order to exhibit the complex nature of interface evolution for longer times, we performed a simulation up to $t = 100$. In this calculation, we start with a small initial ellipse with semiaxes $a = 0.04$, $b = 0.03$. This models the situation where a small twin *nucleates* at the origin and grows subsequently. We add a small isotropic term to the usual anisotropic term in the kinetic relation, by choosing $M_1 = 0.1$, $M_2 = 3$. The term in (4.14) associated with M_1 allows some mobility in the y direction; this is an order of magnitude lower than the mobility in the x direction associated with the anisotropic coefficient M_2. This allows the interface to decrease the energy somewhat faster than in the case $M_1 = 0$ considered above. The load level is set to $k = 0.3$. Results are shown in Fig. 9. Initial evolution up to $t = 8$ is qualitatively very similar to the one shown above in Figs. 2 and 5. The nucleus grows into a flat needle. The only difference is that the initial tips that emerge from the nucleus are slightly more blunted than the cusped tips of Fig. 2. This is entirely due to the M_1 term. By $t = 10$ the emerging tips have reached the boundary and split, and two reentrant tips have moved into the interior. This configuration is almost identical to the one for $t = 8$ in Fig. 5, which corresponded to the same load level, but fully anisotropic kinetics and a larger initial ellipse. At $t = 15$, each of the four tips remaining on the boundary splits once more into two. The four new reentrant tips, however, only move into the interior by a limited amount and almost stop by $t = 25$. In contrast, the two original reentrant tips continue moving toward each other at a faster pace. At some time between $t = 25$ and $t = 30$ they actually meet at the center. They coalesce and a *topological change* takes place: the needle separates completely into *two disjoint regions*. Each of them has four tips on the boundary and two reentrant tips. Further evolution is rather slow, especially after $t = 80$. The two separate needles move slowly away from each other in the y direction. This is facilitated by the presence of the small isotropic kinetic term. Configurations at $t = 95$ and $t = 100$ were virtually indistinguishable when laid on top of each other. The final configuration at $t = 100$ consists of two parallel straight layers, which are split and tapered at the boundary. The distance between the layers is roughly equal to the distance of each from the top and bottom boundaries. The total energy is plotted as a function of time in Fig. 10. The energy starts decaying very slowly by $t = 20$. However, approximately at $t = 27$, it starts decreasing rapidly again; this corresponds to the actual instant of topological change (complete separation into two regions). It is not clear whether the final observed state is close to equilibrium associated with a local energy minimum. It is conceivable that the remaining reentrant tips might move toward each other, and a second complete separation might occur eventually. This would give rise to four disjoint layers. Verification of this would require a very large amount of computational effort, because of the extremely slow evolution observed at the end of the present simulation.

Equilibria of the present dynamic problem correspond to local minima of a nonconvex variational problem. For example, one can let $W(\nabla u) = \min\{W_0(\nabla u), W_1(\nabla u)\}$, with W_0 and W_1 as in (2.1); thus W is a nonconvex two-well function with minima at $\nabla u = (0, 0)$ and $(0, \xi)$. One then seeks to minimize the total stored elastic energy $E\{u\} = \int_\Omega W(\nabla u)\, dA$ over a suitable class of functions u satisfying the boundary condition (6.1). It is well known [10]

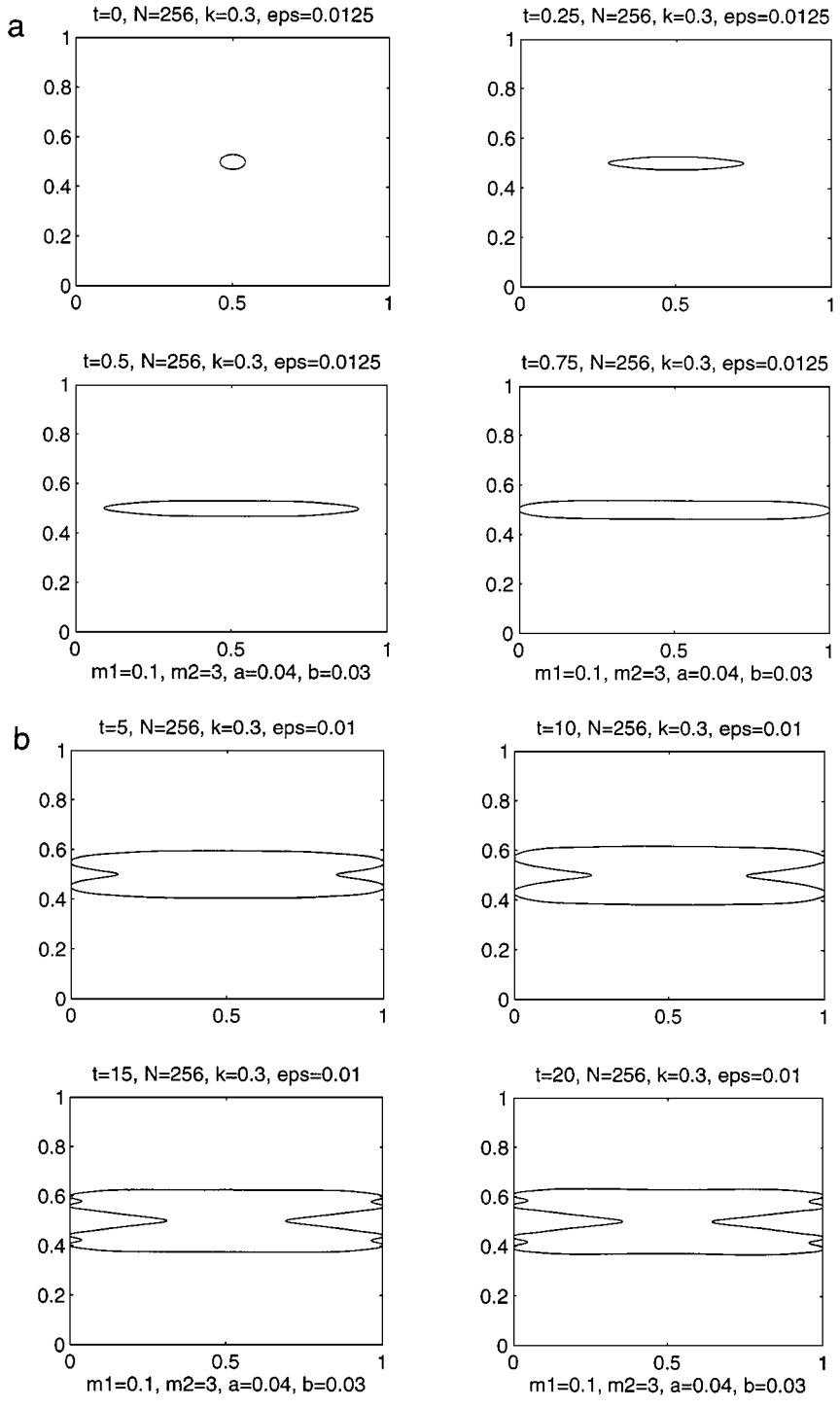

FIG. 9. (a) Sequence of interface configurations starting from a small initial ellipse with $a = 0.04$, $b = 0.03$, with combined kinetics $M_1 = 0.1$, $M_2 = 3$, at load $k = 0.3$. Initial evolution at $t = 0$, 0.25, 0.5, 0.75. (b) Subsequent evolution at $t = 5$, 10, 15, 20. Parameters are as in (a). (c) Subsequent evolution at $t = 25$, 30, 35, 40. Parameters are as in (a). A topological change occurs between $t = 25$ and $t = 30$. (d) Long-time evolution at $t = 50$, 60, 70, 80. Parameters are as in (a).

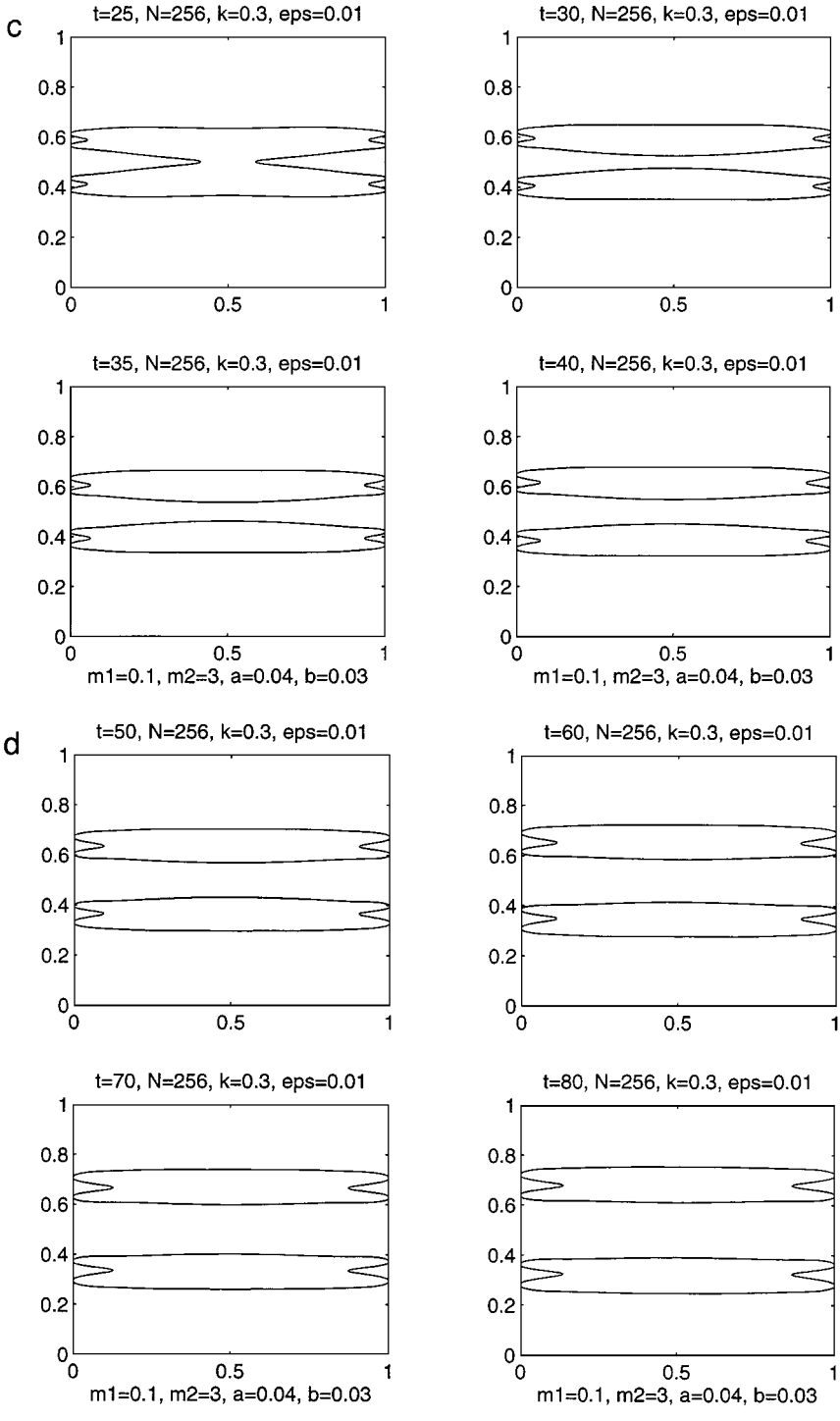

FIG. 9—*Continued*

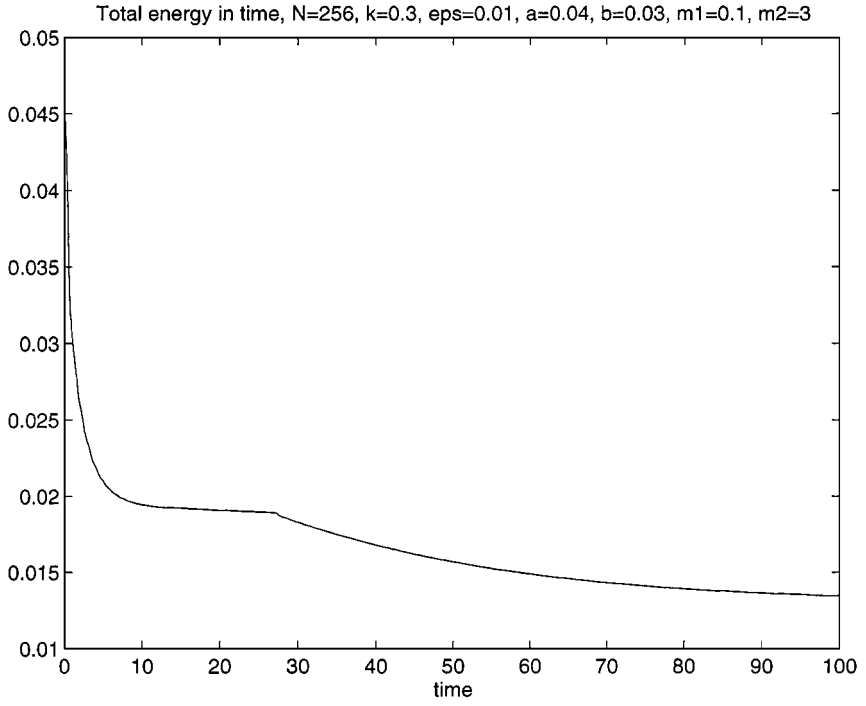

FIG. 10. Total energy versus time for the simulation of Fig. 9 ($k = 0.3$, $M_1 = 0.1$, $M_2 = 3$, $a = 0.04$, $b = 0.03$).

that this problem does not possess a global minimum. This is due to nonconvexity and the incompatibility of the high-strain branch W_1 with the boundary conditions. On the other hand, there are minimizing sequences of functions $\{u_n\}$, for which the energy tends to its infimum value of zero as $n \to \infty$. A typical term of such a sequence is a collection of horizontal layers in the high-strain well with $\nabla u = \xi$, alternating with layers in the low-strain well $\nabla u = (0, 0)$. In particular, u_n is piecewise linear and has n horizontal interfaces. Compatibility with the boundary conditions at the vertical portions of the boundary is achieved by introducing a transition zone or boundary layer, where values of ∇u are not at the two minima of W. This zone penalizes the total energy. However, the size of this zone and thus the total energy approach zero in the limit as $n \to \infty$, while the number of layers grows unbounded. The tapering of needles near the boundary observed in our simulations occurs precisely in order to accommodate the boundary conditions. The latter force the values of u_y at the vertical portions of $\partial\Omega$ to be in the low-strain phase. As a result, a flat high-strain phase layer cannot extend all the way to the boundary. Instead, it tapers into a tip and touches $\partial\Omega$ only at isolated points.

Kohn and Müller [19, 20] consider an alternative model that includes *surface energy* at interfaces. They find equilibria where twin layers branch and taper near the interface. The resulting construction has various similarities with the final configuration encountered in the above simulation. It is interesting to note that Model I adopted here introduces a surface energy term as a consequence of regularization, that however *vanishes in the sharp-interface limit* as $\varepsilon \to 0$. For Model I, the total energy $E(t)$ in (6.3) admits the decomposition $E(t) = E_b(t) + E_s(t)$. The bulk (kinetic plus stored elastic) energy E_b actually equals the total energy associated with Model II (integral of (4.2) over Ω). The surface (interfacial)

energy E_s equals the last term in expression (6.3) of the total energy, namely,

$$E_s(t) = \int_\Omega \frac{1}{2} H_\varepsilon(\varphi)[1 - H_\varepsilon(\varphi)]\, dA. \tag{6.4}$$

This term depends only on the interface configuration through φ and does not involve ∇u. In contrast, the explicit surface energy introduced by Fried and Gurtin [13] depends on the order parameter gradient (analogous to $\nabla\varphi$) and does not vanish in the sharp-interface limit. The integrand in (6.4) is positive inside the transition layer (where $|\varphi| < \varepsilon$) and vanishes elsewhere. Recall that φ is frequently reinitialized to equal signed distance from the interface. As a result, we have the estimate $E_s \approx aL\varepsilon/2$, where L is the total interface length and the constant $a = \int_{-1}^{1} H_1(z)(1 - H_1(z))\, dz \approx 0.2$. Hence, E_s vanishes in the sharp-interface limit as $\varepsilon \to 0$. In our simulations however, E_s typically increases due to interface growth, while E_b decays due to dissipation. Equilibrium is reached when the competition of the two prohibits further decrease of the total energy E. In our last simulation (Fig. 9) with $\varepsilon = 0.01$, at $t = 100$ we have $L \approx 5$ so that $E_s \approx 0.005$, while $E \approx 0.013$ in Fig. 10. A. further separation of two into four needles would almost double E_s, making it comparable to the total energy. As a result, it seems unlikely that any further topological change would take place. We suspect that the final configuration of Fig. 9 at $t = 100$ is very close to equilibrium. Further topological change is presumably possible if ε is decreased; however, that would require a reduction of mesh size from the current value of $h = 1/256$. Model II does not involve surface energy and might allow repeated topological changes were it not for numerical difficulties associated with interface kinetics discussed previously.

7. CONCLUDING REMARKS

The level-set method presented here is efficient in capturing various aspects of the evolution of twinning. As it does not rely on interface tracking and remeshing, it is well suited for the study of complex microstructure formation.

In contrast to other ingredients of the constitutive law, the kinetic relation is very difficult to measure from experiments. The fact that the kinetic relation can be assigned independently in the current scheme is a strong point of the method; it allows comparison and testing of various proposed kinetic models. Here, for instance, we demonstrate that orientation dependence (anisotropy) in the kinetic relation is crucial for prediction of the shape of twin needles. Various other regularized theories lack this flexibility. Regularization due to viscosity and higher gradients fixes a particular type of kinetics that cannot be modified. Generalizations of the kinetics that include, for example, curvature dependence are relatively easy to implement in the present method.

Our results suggest that the energy functional for the corresponding static problem may possess multiple local minima, each with a higher number of disjoint layers, but lower energy. Transition from one such state to another requires an increase in the number of layers, and hence a topological change. Tip splitting, followed by merging of reentrant tips, provides a mechanism for this change. This observation agrees with the conclusions of Abeyaratne *et al.* [1]. The splitting event is a complicated dynamic process that is not fully understood from an analytical viewpoint. Our simulations indicate that it occurs above a critical level of loading.

Our model does not include a specific nucleation criterion analogous to the one adopted by Abeyaratne and Knowles [3]. Thus it cannot predict nucleation of a high-strain zone in a

region entirely in the low-strain phase, and vice versa. It is possible to incorporate a nucleation criterion based on critical levels of strain for each phase, by a suitable modification of the level-set reinitialization scheme.

The method is fully capable of treating multiple phases of different crystal symmetry with three-dimensional kinematics and fully nonlinear stored-energy functions. When so extended, it is directly applicable to the study of the austenite–martensite transitions occurring in specific shape-memory alloys. Thermomechanical coupling, especially important in transitions with substantial latent heat, can also be incorporated. We intend to pursue such issues in later studies.

ACKNOWLEDGMENTS

T.Y.H. acknowledges the support of the Air Force Office of Scientific Research and the National Science Foundation through Grants AFOSR F49620-97-1-0282 and DMS-9704976, respectively. P.R. was partially supported by the National Science Foundation through Grant MSS-9312858. P.G.L. was partially supported by the National Science Foundation through Grants DMS 94-01003 and DMS 95-02766, and a Faculty Early Career Development Award, and also by the Centre National de la Recherche Scientifique, France.

REFERENCES

1. R. Abeyaratne, C. Chu, and R. D. James, Kinetics of materials with wiggly energies: Theory and application to the evolution of twinning microstructures in a Cu–Al–Ni shape-memory alloy, *Phil. Mag. A* **73**, 457 (1996).
2. R. Abeyaratne and J. K. Knowles, On the driving traction acting on a surface of strain discontinuity in a continuum, *J. Mech. Phys. Solids* **38**, 345 (1990).
3. R. Abeyaratne and J. K. Knowles, Kinetic relations and the propagation of phase boundaries in solids, *Arch. Rat. Mech. Anal.* **114**, 119 (1991).
4. R. Abeyaratne and J. K. Knowles, Implications of viscosity and strain gradient effects for the kinetics of propagating phase boundaries in solids, *SIAM J. Appl. Math.* **51**, 1205 (1991).
5. J. Ball, P. J. Holmes, R. D. James, P. L. Pego, and P. J. Swart, On the dynamics of fine structure, *J. Nonlinear Sci.* **1**, 17 (1991).
6. J. Ball and R. D. James, Fine phase mixtures as minimizers of energy, *Arch. Rat. Mech. Anal.* **100**, 13 (1986).
7. G. Caginalp and Y. Nishiura, The existence of travelling waves for phase-field equations and convergence to sharp interface models in the singular limit, *Q. Appl. Math.* **49**, 147 (1991).
8. Y. C. Chang, T. Y. Hou, B. Merriman, and S. J. Osher, A level set formulation of Eulerian interface capturing methods for incompressible fluid flows, *J. Comput. Phys.* **124**, 449 (1996).
9. C. Chu and R. D. James, Biaxial loading experiments on Cu–Al–Ni single crystals, in *Experiments in Smart Materials and Structures*, edited by K.-S. Kim, ASME-AMD, Vol. 181 (1993), p. 61.
10. B. Dacorogna, *Direct Methods in the Calculus of Variations* (Springer-Verlag, Berlin, 1990).
11. H. T. Fan and M. Slemrod, The Riemann problem for systems of conservation laws of mixed type, in *Shock Induces Transitions and Phase Structures in General Media*, edited by R. Fosdick, E. Dunn, and H. Slemrod, IMA, Vol. Math. Appl. 52 (Springer-Verlag, Berlin/New York, 1993), p. 61.
12. E. Fried, Stability of a two-phase process in an elastic solid, *J. Elasticity* **31**, 163 (1993).
13. E. Fried and M. E. Gurtin, Dynamics solid–solid transitions with phase characterized by an order parameter, *Physica D* **72**, 287 (1994).
14. J. Glimm, E. Isaacson, D. Marchesin, and O. A. McBryan, Front tracking for hyperbolic systems, *Adv. Appl. Math.* **2**, 91 (1981).
15. M. E. Gurtin and A. Struthers, Multiphase thermomechanics with interfacial structure 3: Evolving phase boundaries in the presence of bulk deformation, *Arch. Rat. Mech. Anal.* **112**, 97 (1990).
16. B. T. Hayes and P. G. LeFloch, Non-classical shocks and kinetic relations: Scalar conservation laws, *Arch. Rat. Mech. Anal.* **139**, 1 (1997).

17. R. D. James, The propagation of phase boundaries in elastic bars, *Arch. Rat. Mech. Anal.* **73**, 125 (1980).
18. R. V. Kohn, The relaxation of a double-well energy, *Continuum Mech. Thermodyn.* **3**, 193 (1991).
19. R. V. Kohn and S. Müller, Branching of twins near an austenite-twinned martensite interface, *Phil. Mag. A* **66**, 697 (1992).
20. R. V. Kohn and S. Müller, Surface energy and microstructure in coherent phase transitions, *Comm. Pure Appl. Math.* **47**, 405 (1994).
21. P. G. LeFloch, Propagating phase boundaries: Formulation of the problem and existence via Glimm's scheme, *Arch. Rat. Mech. Anal.* **123**, 153 (1993).
22. R. J. LeVeque and K. M. Shyue, *Shock Tracking Based on High Resolution Wave Propagation Methods*, Research Report 91-02, ETH, Zurich (1991).
23. T. P. Liu and K. Zumbrun, On nonlinear stability of general undercompressive viscous shock waves, *Comm. Math. Phys.* **174**, 319 (1995).
24. M. Luskin, Approximation of a laminated microstructure for a rotationally invariant, double well energy density, *Numer. Math.* **75**, 205 (1996).
25. S. J. Osher and J.A. Sethian, Fronts propagating with curvature dependent speed: Algorithms based on Hamilton–Jacobi formulation, *J. Comput. Phys.* **79**, 12 (1988).
26. P. Rosakis, Compact zones of shear transformation in an anisotropic solid, *J. Mech. Phys. Solids* **40**, 1163 (1992).
27. P. Rosakis and H. Y. Tsai, On the role of shear instability in the modeling of crystal twinning, *Mech. Mater.* **17**, 245 (1994).
28. P. Rosakis and H. Y. Tsai, Dynamic twinning processes in crystals, *Intl. J. Solids Struct.* **33**, 2711 (1995).
29. S. A. Silling, Dynamic growth of martensitic plates in an elastic material, *J. Elasticity* **28**, 143 (1992).
30. M. Sussman, P. Smereka, and S. J. Osher, A level-set approach for computing solutions to incompressible two-phase flow, *J. Comput. Phys.* **114**, 146 (1994).
31. P. J. Swart and P. J. Holmes, Energy minimization and the formation of microstructure in dynamic antiplane shear, *Arch. Rat. Mech. Anal.* **121**, 37 (1992).
32. L. Truskinovsky, Structure of an isothermal phase discontinuity, *Sov. Phys. Dokl.* **30**, 945 (1985).
33. L. Truskinovsky, Kinks versus shocks, in *Shock Induced Transitions and Phase Structures in General Media*, edited by R. Fosdick, E. Dunn, and H. Slemrod (Springer-Verlag, Berlin/New York, 1991), p. 185.
34. H. Y. Tsai, *Mechanics of Deformation Twinning*, Ph.D. thesis, Cornell University (1994).
35. H. Tsai and P. Rosakis, On anisotropic compressible materials that can sustain dynamic anti-plane shear, *J. Elasticity* **35**, 213 (1994).
36. D. F. Williams and C. N. Reid, A dynamic study of twin-induced brittle fracture, *Acta Metallurgica* **19**, 931 (1971).
37. X. G. Zhong, T. Y. Hou, and P. G. LeFloch, Computational methods for propagating phase boundaries, *J. Comput. Phys.* **124**, 192 (1996).